

COLORADO STATE UNIVERSITY

August 20, 2004

WE HEREBY RECOMMEND THAT THE THESIS PREPARED UNDER OUR
SUPERVISION BY AMANDA ANDERSON ENTITLED

“CHARACTERIZATION OF THE NEUTRON SPECTRUM EMITTED FROM
CONCEALED WEAPONS GRADE NUCLEAR MATERIALS”

BE ACCEPTED AS FULFILLING IN PART REQUIREMENTS FOR THE DEGREE
OF MASTER OF SCIENCE.

Committee on Graduate Work

Kirk Hallahan, PhD.

John E. Pinder, PhD.

Thomas B. Borak, PhD., **Advisor**

John A. Zimbrick, PhD., **Department Head**

ABSTRACT OF THESIS

CHARACTERIZATION OF THE NEUTRON SPECTRUM EMITTED FROM CONCEALED WEAPONS GRADE NUCLEAR MATERIALS

The purpose of this project is to evaluate the neutron spectrum emitted by concealed weapons grade nuclear material. A source of highly enriched uranium (HEU) was modeled in several different configurations. The geometry of the source volume was varied as well as the dimensions of the shielding material. The configurations were modeled with the Monte Carlo N-Particle Transport (MCNP) code. The results in the form of cumulative energy distributions were compared for neutrons crossing a surface at less than 1.0×10^{-3} MeV. Through use of varying source geometries, densities, sizes, and shielding configurations it was determined that neutron shielding would cause the greatest difference between the cumulative distribution curves.

Amanda Anderson, LT, USNR, MSC
Department of Environmental and Radiological Health Sciences
Colorado State University
Fort Collins, CO 80523
Summer 2004

TABLE OF CONTENTS

List of Tables and Figures v

Introduction 1

Definitions 1

Areas of Vulnerability 3

History of Threat 4

Materials and Methods 6

MCNP Computer Modeling 6

Precision and Accuracy in MCNP 10

MCNP Statistical Output 12

Comparison of Neutron Energy Spectra 14

MCNP Geometry Verifications 14

Results and Discussion 20

Conclusion 44

Summary of Results 44

Future Research 47

Bibliography 51

Appendix A: Classification of Neutrons 54

Appendix B: Material Composition 55

Appendix C: Relative Error of Neutron Current Tables 56

LIST OF TABLES AND FIGURES

TABLES

Table 1	Comparison of Cumulative Distributions for 500 g, HEU, Unshielded, Uniform Cylinder, Sphere, and Sheet Sources and a Points Source With a Watt Spectrum Distribution 23
Table 2	Comparison of Cumulative Distributions 500 g, HEU, Uniform Sphere Source Unshielded, with 5 cm of Polyethylene, with 10 cm of Polyethylene, with 15 cm of Polyethylene, with 20 cm Polyethylene Shielding 26
Table 3	Comparison of Cumulative Distributions for a 500 g and a 2000 g, HEU, Unshielded, Uniform Cylinder Source 27
Table 4	Comparison of Cumulative Distributions for a 500 g and a 2000 g, HEU, Unshielded, Uniform Sheet Source 29
Table 5	Comparison of Cumulative Distributions of X + Y axes vs. Z axis for 500 g, HEU Cylinder Source, Unshielded, 30
Table 6	Comparison of Cumulative Distributions of Y + Z axes vs. X axis for 500 g, HEU Sheet Source, Unshielded, 32
Table 7	Comparison of Cumulative Distributions of X, Y and Z axes for 500 g, HEU Cylinder Source with 7.5 x 20 x 15 cm of Polyethylene Shielding 34
Table 8	Comparison of Cumulative Distributions of X, Y and Z axes for 500 g, HEU Cylinder Source with 24 x 7 x 28 cm of Polyethylene Shielding 37
Table 9	Comparison of Cumulative Distributions for 500 g, HEU Cylinder, Source Along the X axis with 7.5 x 20 x 15 cm of Polyethylene Shielding and with 24 x 7 x 28 cm of Polyethylene Shielding 38
Table 10	Comparison of Cumulative Distributions for 500 g, HEU Sheet Source with 7.5 x 20 x 15 cm of Polyethylene Shielding 40
Table 11	Comparison of Cumulative Distributions for 500 g, HEU Sheet Source with 24 x 7 x 28 cm of Polyethylene Shielding 42

Table C-1	Relative Error, Neutron Tracking Data, 500 g, HEU, Uniform Cylinder, Sheet, and Sphere Sources and Point Source with Watt Spectrum Distribution, No Shielding 56
Table C-2	Relative Error, Neutron Tracking Data, 500 g, HEU Sphere, Unshielded, with 5 cm of Polyethylene, with 10 cm of Polyethylene, with 15 cm of Polyethylene, and with 20 cm Polyethylene 57
Table C-3	Relative Error, Neutron Tracking Data, 500 g, HEU Cylinder Source, Unshielded, X + Y axes and Z axis 58
Table C-4	Relative Error, Neutron Tracking Data, 500 g, HEU Sheet Source, Unshielded, Y + Z axes and X axis 59
Table C-5	Relative Error, Neutron Tracking Data, 500 g, HEU Cylinder, Surrounded by 7.5 x 20 x 15 cm Polyethylene, X, Y and Z axes 60
Table C-6	Relative Error, Neutron Tracking Data, 500 g, HEU Cylinder, Surrounded by 24 x 7 x 28 cm Polyethylene, X, Y and Z axes 61
Table C-7	Relative Error, Neutron Tracking Data, 500 g, HEU Sheet, Surrounded by 7.5 x 20 x 15 cm Polyethylene, X, Y and Z axes 62
Table C-8	Relative Error, Neutron Tracking Data, 500 g, HEU Sheet Surrounded by 24 x 12 x 28 cm Polyethylene 63

FIGURES

Figure 1	Neutron Current Crossing 10 Spheres, Monoenergetic Point Source 15
Figure 2	Neutron Current Crossing 10 Spheres, Monoenergetic Point Source Surrounded by 1 cm of Aluminum 16
Figure 3	Neutron Current Crossing the 10 cm Sphere, Discrete Energy Distribution 17
Figure 4	Cumulative Distribution of Theoretical Watt Fission Spectrum vs. Calculated Watt Fission Spectrum 18
Figure 5	Neutron Current Emitted From Uniformly Distributed HEU Cylinder, Sheet, and Sphere Sources, 500 g, at the 200 cm Empty Sphere Surface, 19
Figure 6	Configuration of a Uniform Cylinder of HEU, 500 g, Surrounded by Six Detectors 20

- Figure 7 Configuration of a Uniform Sheet of HEU, 500 g, Surrounded by Six Detectors **21**
- Figure 8 Configuration of a Uniform Sphere of HEU, 500 g, Surrounded by Six Detectors **21**
- Figure 9 Cumulative Distribution Comparison of 500 g HEU, Uniform Cylinder, Sheet, Sphere, and Watt Point Sources, No Shielding **22**
- Figure 10 Configuration of a Uniform Sphere of HEU, 500 g, Unshielded and Surrounded by 5 cm of Polyethylene, 10 cm of Polyethylene, and 15 cm of Polyethylene, and 20 cm of Polyethylene **24**
- Figure 11 Cumulative Distribution Comparison of Configuration of a Uniform Sphere of HEU, 500 g, Unshielded and Surrounded by 5 cm of Polyethylene, 10 cm of Polyethylene, and 15 cm of Polyethylene, and 20 cm of Polyethylene **25**
- Figure 12 Cumulative Distribution Comparison of 500 g & 2000g HEU, Uniform Cylinder Source, No Shielding **27**
- Figure 13 Cumulative Distribution Comparison of 500 g & 2000g HEU, Uniform Sheet Source, No Shielding **28**
- Figure 14 Cumulative Distribution Comparison of X + Y and Z axes, 500 g HEU, Uniform Cylinder Source, Unshielded **29**
- Figure 15 Cumulative Distribution Comparison of Y + Z and X axes, 500 g HEU, Uniform Sheet Source, Unshielded **31**
- Figure 16 Configuration of a Uniform Cylinder of HEU, 500 g, Surrounded by 7.5 x 20 x 15 cm Polyethylene and Six Detectors **33**
- Figure 17 Cumulative Distribution Comparison of X, Y, and Z Axes, 500 g HEU, Uniform Cylinder Source, Surrounded by 7.5 x 20 x 15 cm Polyethylene **34**
- Figure 18 Configuration of a Uniform Cylinder of HEU, 500 g, Surrounded by 24 x 7 x 28 cm Polyethylene and Six Detectors **35**
- Figure 19 Cumulative Distribution Comparison of X, Y, and Z Axes, 500 g HEU, Uniform Cylinder Source, Surrounded by 24 x 7 x 28 cm Polyethylene **36**

- Figure 20 Cumulative Distribution Comparison of X Axes, 500 g HEU, Uniform Cylinder Source Surrounded by 7.5 x 20 x 15 cm and Uniform Cylinder Source Surrounded by 24 x 7 x 28 cm Polyethylene **37**
- Figure 21 Configuration of a Uniform Sheet of HEU, 500 g, Surrounded by 7.5 x 20 x 15 cm Polyethylene and Six Detectors **38**
- Figure 22 Cumulative Distribution Comparison of X, Y, and Z Axes, 500 g HEU, Uniform Sheet Source Surrounded by 7.5 x 20 x 15 cm Polyethylene **39**
- Figure 23 Configuration of a Uniform Sheet of HEU, 500 g, Surrounded by 24 x 12 x 28 cm Polyethylene and Six Detectors **41**
- Figure 24 Cumulative Distribution Comparison of X, Y, and Z Axes, 500 g HEU, Uniform Sheet Source Surrounded by 24 x 7 x 28 cm Polyethylene **42**
- Figure 25 Cumulative Distribution Comparison of X and Y Axes, 500 g HEU, Uniform Cylinder and Sheet Source Surrounded by 7.5 x 20 x 15 cm Polyethylene and Uniform Cylinder and Sheet Source Surrounded by 24 x 12 x 28 cm Polyethylene **43**

INTRODUCTION

The nation's interest in nuclear security has increased dramatically over the past few years. There are two different aspects to these concerns; First there is the threat of radiological dispersal devices (RDD), often referred to in the media as 'dirty bombs'. The second threat revolves around improvised nuclear devices (IND) otherwise known as weapons of mass destruction (WMD). This project focuses on the latter issue. The purpose of this project is to characterize the neutron spectrum emitted from weapons grade uranium and plutonium that would be emitted from a shielded suitcase or cargo container. By characterizing the likely spectrum that would be emitted in such a scenario, a more efficient and practical neutron detector could be designed and implemented throughout ports of entry in the United States to quickly identify suspicious cargo, while reducing the impact of inspections on commerce.

Definitions

Before discussing the materials used to create INDs, it is important to present on a few definitions. Of particular interest is the difference in defining materials in the United States and in Russia. These differences have on occasion led to some confusion from accountability reports from the nuclear arsenal of the former Soviet Union. The Russian government reports that they have had no instances of theft of weapons grade material. This is because they define *weapons grade material* as uranium that is enriched to greater than 90% ^{235}U , and Plutonium enriched to greater than 93% ^{239}Pu (Stern, 2000). They make little mention of incidents involving the theft of *weapons usable material* which the

Russians define as uranium that is enriched to greater than 20% ^{235}U (Stern, 2000).

Given that the Russian government reports that no cases involving the smuggling of weapons grade material from the former Soviet Union have occurred, this is an important distinction.

Fission is a process in which a heavy nucleus splits into two nuclei of intermediate mass numbers. A number of fission fragments, prompt gamma rays, and 2-3 neutrons are released when fission occurs. Fission neutrons contribute approximately 5 MeV to the total energy released during a fission (Glasstone and Sesonske, 1991). The neutrons emitted from fission can survive long enough to lose sufficient energy and become thermalized. If a thermal neutron is then captured by another nucleus, it can create enough instability within the nucleus to cause another fission to occur. This chain reaction can lead to criticality. *Criticality* is a condition such that for each fission, at least one neutron survives to produce another fission (Glasstone and Sesonske, 1991).

Fissile material consists of nuclides in which fission can be induced by thermal neutrons. These materials include ^{233}U , ^{235}U , ^{239}Pu , and ^{241}Pu (Duderstadt and Hamilton, 1976). The most common elements and the most likely to be used in a nuclear device are ^{235}U and ^{239}Pu . In order to achieve criticality, an adequate amount of fissile material must be present, and it must have the appropriate geometry and density. The amount of fissile material needed to achieve criticality is referred to as *critical mass*.

Nuclides in which fission can be induced with more energetic or fast neutrons, are called *fissionable material*. These nuclides include ^{232}Th , ^{238}U , ^{240}Pu (Duderstadt and Hamilton, 1976). These materials can not be used to sustain criticality.

Areas of vulnerability

According to the U.S. Customs service there are currently 317 official ports of entry in the United States (Department of Homeland Security, 2003, Ports of Entry). Every year approximately 200 million sea cargo containers are shipped worldwide (Department of Homeland Security, 2003, Container Security Initiative). The U.S. Customs and Border Protection (CBP) process is a first line of defense in preventing nuclear material from entering the United States illegally.

The Container Security Initiative (CSI) was established through the CBP, January 2002, to prevent containerized cargo from being exploited by terrorists (Department of Homeland Security, 2003, Container Security Initiative). One objective of this initiative is to “use technology to *quickly* pre-screen high-risk containers.” (Department of Homeland Security, 2003, U.S. Customs and Border Protection Response to Terrorism).

Another area of vulnerability exists at airports. It is possible but less likely that someone would try to smuggle nuclear material through an airport. The nature of airport screening allows inspectors more time with each piece of checked baggage. It is not as practical for customs inspectors at other ports of entry to allot as much inspection time for every container that passes through a port. The objective of this research is to characterize a neutron spectrum that could be used for these detection purposes.

History of the threat

Recently, Russia has placed greater emphasis on nuclear security, due in part to the September 11, 2001 terrorist attacks and cooperative efforts with the United States;

however, there is still unresolved concern centering around unaccounted for nuclear material from the Soviet Union era. Several incidents have occurred since the break-up of the Soviet Union, which have fostered some apprehension. In 1992, 1.5 Kg of weapons grade uranium was reported stolen from the Luch Production Association (National Intelligence Council [NIC], 2002). Following that, in 1994, 3.0 Kg of weapons grade uranium was stolen in Moscow (NIC, 2002).

In 1997, General Alexander Lebed testified to members of the U.S. Congress that 84 'RA-115 suitcase bombs' were missing from the Russian arsenal. These suitcases contain nuclear bombs, weigh 30 Kilograms, and have an explosive yield of approximately 2 Kilotons (Stern, 2000). They can easily be activated by one person.

In 1999, 4.0 grams of highly enriched uranium (HEU), suspected to have originated from Russia, was seized in Bulgaria (NIC, 2002). The National Intelligence Council (NIC) suspects that undetected smuggling of Soviet era nuclear material has occurred and they have expressed concern to Congress about the amount of material that could have been smuggled over the past 10 years (NIC, 2002).

A discovery of large stockpiles of beryllium found in Lithuania in 1993 has also caused some alarm (Stern, 2000). Although beryllium is not a fissile material, it can be used as an effective neutron reflector. This type of material could be used to encase a core of fissile material. The reflective property would improve a criticality reaction, and allow for a smaller quantity of fissile material to be used. After this discovery, it was determined that a client from Switzerland had already been identified as a buyer of the material.

MATERIALS AND METHODS

MCNP Computer Modeling.

The neutrons emitted from a possible container are characterized using the Monte Carlo N-Particle Transport (MCNP) computer code created by Los Alamos National Laboratory (Department of Energy and University of California at Los Alamos National Laboratory, 2001). This computer code allows the user to create a three dimensional geometry and define a source of radiation. The output provides various particle information, including particle flux, number of particles captured in the material, and number of particles escaped from the material (Briesmeister, 2000).

The computer program is so named because it operates on a Monte-Carlo type process. Instead of using one mathematical formula to calculate the probability distribution of a particle track, a game of 'Russian Roulette' is used. Every time a particle moves into a new cell, it is assigned a value of 1 or 0. If it is given a value of 0, the history is terminated. If it is assigned a value of 1, the position, time, and energy is tallied and the process starts over. This method was first used in 1947 to model neutron diffusion and multiplication models for nuclear weapons. MCNP represents a computer code that has evolved since the late 1940s (Briesmeister, 2000). Version 4C was used in this project. It has been updated with ENDF neutron cross section libraries. These libraries are created from extensive experimental analysis of measurements of neutron cross sections (Duderstadt and Hamilton, 1976). Any necessary interpolation during the running of a program will have an error tolerance of <1% (Briesmeister, 2000). The probability of a first collision for a particle between l and $l + dl$ is defined by:

$$p(l)dl = e^{-\Sigma_t l} \Sigma_t dl \quad (\text{Equation 1}) \quad (\text{Briesmseister, 2000})$$

$p(l)dl = \text{probability a particle collision will occur between } l \text{ and } l+dl$

$\Sigma_t = \text{total macroscopic cross section of target material interpreted as}$

$\text{probability per unit length of a collision}$

In the MCNP computer code each neutron is analyzed at every cell of travel.

When a neutron is emitted from the source the code will assign a value of 1 or 0 to it, as previously described, which determines what the neutron will do next. This happens with every interaction of the neutron until it escapes or falls below the cutoff energy (Briesmseister, 2000). The energy cutoff used in this project is 1×10^{-6} MeV. MCNP will track neutrons with a maximum energy of 20 MeV. MCNP provides an output of the neutron tallies in which the tallies are normalized to 1 starting particle and integrated over user specified energy bins.

During the life of the neutron it may fall below the cutoff energy, become captured in another nucleus, or interact by either elastic or inelastic scatter. When an interaction occurs the following relationship is used to determine the probability that it will be an elastic collision.

$$\frac{\sigma_{el}}{\sigma_{in} + \sigma_{el}} = \frac{\sigma_{el}}{\sigma_T - \sigma_a} \quad (\text{Equation 2}) \quad (\text{Briesmseister, 2000})$$

σ_{el} = elastic cross section of material

σ_{in} = inelastic cross section of material

σ_a = adsorption cross section of material

$\sigma_T = \sigma_a + \sigma_{in}$ = total cross section of material

The selection of inelastic scatter is made with the remaining probability:

$$\frac{\sigma_{in}}{\sigma_T - \sigma_a} \quad \text{(Equation 3) (Briesmseister, 2000)}$$

Fast neutrons (Appendix A) mostly lose energy by elastic scatter. During elastic scatter, kinetic energy is conserved (Turner, 1986). As neutron energy decreases, probability of absorption by the target nucleus increases. A neutron will eventually lose enough energy to become a thermal neutron (Appendix A). Once a neutron becomes thermalized, it will continue to travel randomly until it becomes absorbed by a nucleus. This typically is the most dominant process of neutron moderation or the slowing of neutron particles (Turner, 1986). The MCNP computer program calculates the energy of each elastic scatter neutron through equation 4.

$$E_{out} = \frac{1}{2} E_{in} [(1 - \alpha)\mu_{cm} + 1 + \alpha]$$
$$\alpha = \left(\frac{A-1}{A+1} \right)^2$$

(Equation 4) (Briesmseister, 2000)

E_{in} = incident neutron energy

μ_{cm} = center-of-mass cosine of angle between incident and exit particle direction

A = mass of target nuclide

During inelastic scatter, the target nucleus will only absorb some energy and it will be left in an excited state (Turner, 1986). Inelastic scatter may consist of any of the following types of reactions: (n, n'), (n, 2n), (n, f), (n, n' α). The energy equation used for inelastic scatter is as follows:

$$E_{out} = E_{out_{cm}} + \left[\frac{E_{in} + 2\mu_{cm}(A+1)\sqrt{E_{in}E_{out_{cm}}}}{(A+1)^2} \right] \quad \text{(Equation 5) (Briesmseister, 2000)}$$

E_{out} = exit energy

E_{in} = incident neutron energy

$$\alpha = \left(\frac{A-1}{A+1} \right)^2$$

A = mass of target nuclide

μ_{cm} = center-of-mass cosine of angle between incident and exit particle direction

The nucleus may also emit a gamma ray; However gamma rays are very abundant in the natural environment. In other words, gamma rays emitted from small amounts of weapons grade fissile material will probably be attenuated by and most likely indistinguishable from background radiation.

Precision and Accuracy in MCNP.

Accuracy. Two aspects of the output tallies must be considered. These are precision and accuracy. In this project, accuracy represents the difference between the calculated neutron current across a surface and the true physical quantity. MCNP does not provide accuracy measurements. It is a computer code that has been tested over many years and proven to provide reliable information, but the accuracy of the output is dependent on correct use of the code. The accuracy of the MCNP output for the purposes of this project was previously evaluated by Craig Bias, Major, USAF, BSC. He compared the calculated tallies to measurements with a PuBe source and a LND 201 BF₃ detector (Bias, 2002). These experiments showed that MCNP would provide reliable output for this project. There are, however, three major factors that could affect the accuracy of the output: 1. Code, 2. Problem modeling, and 3. User input (Briesmseister, 2000).

Inherent in the computer code are uncertainties of transport and reaction cross sections and physical constants (Briesmseister, 2000). MCNP uses the most accurate information available. The manner in which a problem is defined in MCNP can also impact the accuracy of the output if inadequate energy and angular distributions are used. Problems for this project were modeled over a wide range of energy, 1×10^{-6} MeV- 10 MeV. To reduce errors caused by angular distributions, programs were always run over a complete angular distribution as well as large neutron particle histories, at the expense of longer computer run times.

Geometry descriptions can also affect the tally accuracy (Briesmseister, 2000). The more complicated the shape of the source and target, the more particle histories will be required for reliable tallies. A sphere inside of a sphere requires far less particle

histories than a box inside a box. The physical characteristics of the materials will affect accuracy as well (Briesmseister, 2000). A material with a higher content of an element such as hydrogen will require much larger neutron particle history inputs than other types of materials. This is because hydrogen has a large neutron cross section. Hydrogen is the most efficient material for slowing down or thermalizing neutrons. A material with a high hydrogen content will have a large number of elastic collisions. As the number of collisions increase, the accuracy decreases. This can be mitigated with a greater number of neutron histories.

User inputs will also affect the accuracy of the output through improper use of particle weighting techniques and erroneous code inputs (Briesmseister, 2000). Particle weighting can be used to reduce computer run-time, however, it was not used for this project, so it will not have an impact on the tally accuracy. Proper use of computer code was first evaluated by running an MCNP sample problem from the MCNP user manual. Once the output was verified, different geometries were evaluated starting with basic geometries and increasing the complexness of the model in increments. All geometries were checked with the geometry plot function. MCNP does not provide an accuracy calculation, so it is important to fully understand the inputs made and study the output tallies carefully.

Precision. Precision is defined in MCNP as the uncertainty of particle tallies caused by statistical fluctuations (Briesmseister, 2000). Precision is affected by 1. Forward vs. adjoint calculations, 2. Tally type, and 3. Number of neutron particle histories. A forward calculation follows a particle from source to detector. An adjoint calculation follows a particle from detector to source. This type of calculation is used for

very small detector surfaces. It is less accurate and can not be used on a continuous energy spectrum. It should not be used unless absolutely necessary. The detector surfaces in this project are 50 cm x 50 cm. Only forward calculations were used.

Tally type is another factor to consider. The smaller the region which is tallied, the more difficult it will be to achieve precision. The ideal tally surface would be a sphere, however, it would not be a practical real-world solution. A more realistic solution would be to set-up detector surfaces on the walls, ceilings and floors of a facility. A surface size of less than 50 cm x 50 cm is not recommended for this project.

The number of particle histories tracked is one obvious factor in tally precision. Precision is proportional to number of particle histories (Briesmseister, 2000). The limiting factor on number of particle histories tracked is computer run time. Very large particle histories are costly in computer run time. In this project, the statistical output determined how many particles needed to be tracked.

MCNP Statistical Output.

It is important when using MCNP to analyze the statistics provided in the output tally. The output provides a relative error calculation as defined by equation 6.

$$R = \frac{S_{\bar{x}}}{\bar{x}} \quad \text{(Equation 6) (Briesmseister, 2000)}$$

$S_{\bar{x}}$ = *standard deviation of the neutron histories in a specified energy bin*

\bar{x} = *average number of neutrons crossing in a specified energy bin*

x = *neutron crossing in specified energy bin*

Anything with a relative error of less than 10% for this project is considered reliable (Briesmseister, 2000). Output with a relative error in the range of 10-20% is questionable (Briesmseister, 2000). Output tallies with an error of greater than 20% were seldom used.

Figure of merit (FOM) information is also provided in the output. This is defined as:

$$FOM = \frac{1}{R^2 T} \quad T = \text{computer time} \quad (\text{Equation 7}) \quad (\text{Briesmseister, 2000})$$

A good tally will have a FOM that approaches a constant value (Briesmseister, 2000).

Variance of variance (VOV) is another statistical check provided with the tally output. VOV indicates the variance of the relative error and indicates tally fluctuations (Briesmseister, 2000). It is defined as:

$$VOV = \frac{S^2(S_x^2)}{S_x^4} = \frac{S^2}{S_x^2} \quad (\text{Equation 8}) \quad (\text{Briesmseister, 2000})$$

$$S^2(S_x^2) = \text{estimation of variance of } S_x^2$$

$$S_x^2 = \text{estimation of } \bar{x}$$

VOV should be less than 10% for all problems (Briesmseister, 2000).

Comparison of Neutron Energy Spectra.

The goal of this project was to characterize the neutron spectra emitted from concealed weapons grade material for the purpose of designing an efficient detector that could be used at ports of entry around the United States. Whether or not the spectra are statistically different is irrelevant at this point. Cumulative distribution curves are instead

developed for the different configurations and then compared at the 1×10^{-3} MeV point. The percent of neutrons crossing a detector surface less than or equal to 1×10^{-3} MeV is quantified for every configuration. The data collected with MCNP was collected for the following energy bins: $0 - 1 \times 10^{-6}$ MeV, $1 \times 10^{-6} - 3 \times 10^{-6}$ MeV, $3 \times 10^{-6} - 1 \times 10^{-5}$ MeV, $3 \times 10^{-5} - 1 \times 10^{-4}$ MeV, $1 \times 10^{-5} - 3 \times 10^{-5}$ MeV, $1 \times 10^{-4} - 3 \times 10^{-4}$ MeV, $3 \times 10^{-4} - 1 \times 10^{-3}$ MeV, $1 \times 10^{-3} - 3 \times 10^{-3}$ MeV, $3 \times 10^{-3} - 1 \times 10^{-2}$ MeV, $1 \times 10^{-2} - 3 \times 10^{-2}$ MeV, $3 \times 10^{-2} - 1 \times 10^{-1}$ MeV, $1 \times 10^{-1} - 3 \times 10^{-1}$ MeV, $3 \times 10^{-1} - 1.0$ MeV, $1.0 - 3.0$ MeV, $3.0 - 10.0$ MeV. Relative error for all of the neutron tracking histories is also shown in Appendix C. This is an important part of the data collected because it provides an indication of where in the energy ranges of the various configurations more efficient detection can be accomplished.

MCNP Geometry Verifications.

The geometry function of MCNP was first checked by running a sample problem from the MCNP manual, and then running simple geometry problems using a point source with a uniform distribution. A configuration using a monoenergetic point source inside ten empty spheres verified the geometry function was working correctly. The results are indicated in Figure 1.

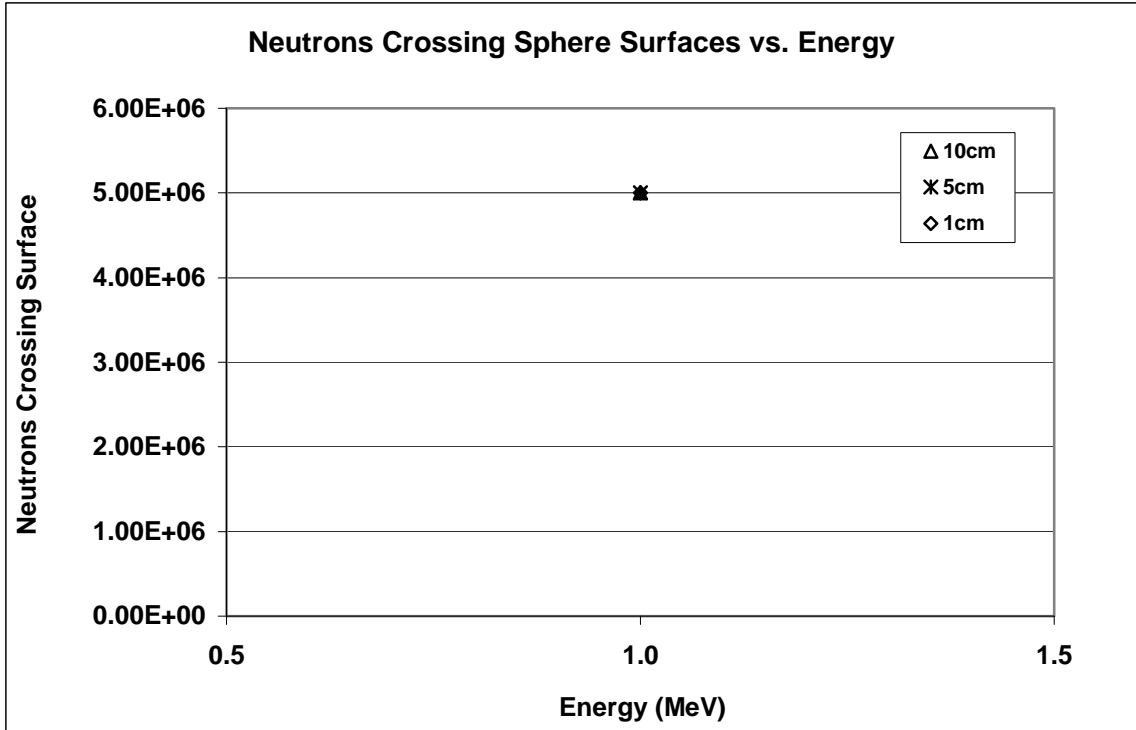


Figure 1. Number of neutrons crossing each sphere surface with a radius of 1 cm, 5cm, and 10cm. Neutrons were emitted from a point source of 1 MeV inside the empty spheres. Output is derived from a MCNP program using 5,000,000 neutron histories. Only one point is displayed on the graph as all other energy bins were found to have zero neutron histories.

The material input functional of MCNP was verified next. The same monoenergetic point source was modeled with a 1 cm sphere of Al surrounding it. This output indicated a peak at 1.0 MeV along with a few neutrons crossing the surface at slightly lower energies (Figure 2). These were the expected results as 1 cm of Al will not moderate neutrons extensively.

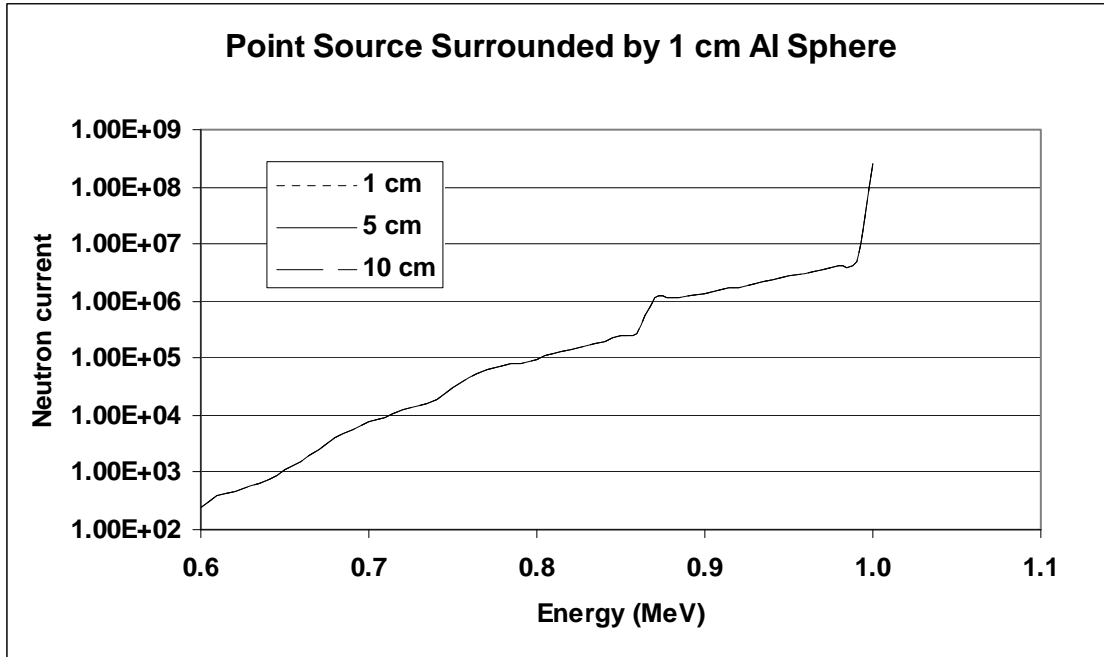


Figure 2. Number of neutrons crossing each sphere surface. Neutrons were emitted from a point source of 1 MeV inside of a 1 cm radius Aluminum sphere which was then surrounded by two empty spheres with radii of 5 cm and 10 cm. Output is derived from MCNP program using 290,000,000 neutron histories. Neutron track histories less than 0.6 MeV were not included because R was greater than 10%.

Once the material input function was verified as accurate, the energy distribution input function was tested. The tested distribution consisted of four discrete energies occurring at 0.8 MeV, 0.9 MeV, 1.0 MeV and 1.1 MeV. The corresponding probability density distribution is 12.5%, 25%, 50%, and 12.5%. In this model, there was no intermediate moderating material, so the expected output is 625,000 neutrons crossing at 0.8 MeV, 1,125,000 neutrons crossing at 0.9 MeV, 2,500,000 neutrons crossing at 1.0 MeV, and 625,000 neutrons crossing at 1.1 MeV. The actual results, shown in Figure 3, concur with the expected results.

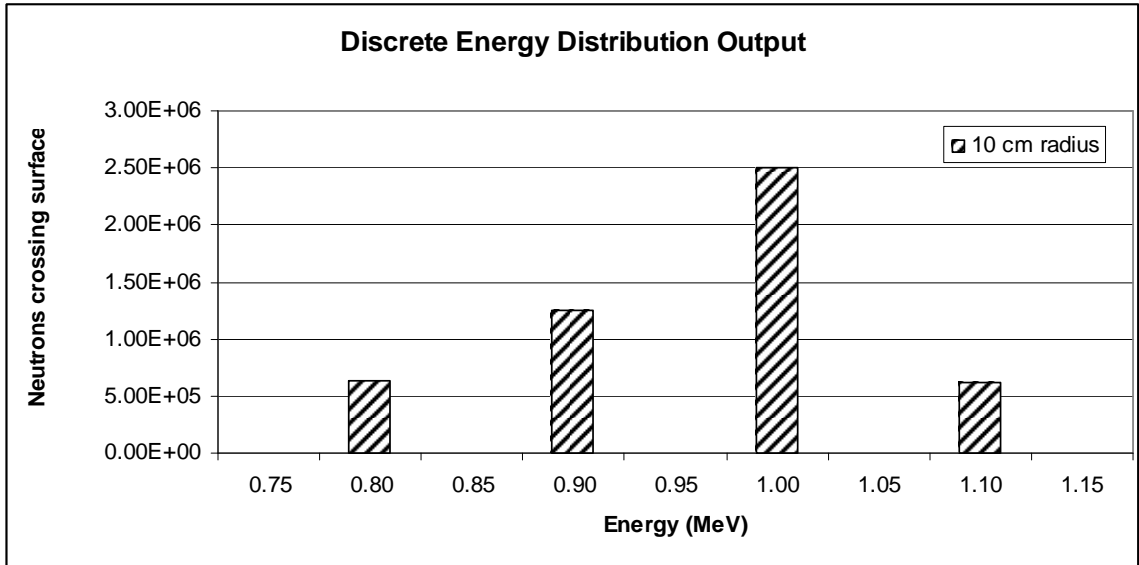


Figure 3. Number of neutrons crossing each sphere surface. Neutrons were emitted from a point source with a discrete energy distribution of 0.8 MeV, 0.9 MeV, 1.0 MeV, 1.1 MeV at a corresponding probability distribution of 12.5%, 25%, 50%, and 12.5%. The neutron track histories shown are measured at a 10 cm empty sphere. Output is derived from MCNP program using 5,000,000 neutron histories.

MCNP also has various defined energy spectra. These include the Gaussian, Maxwellian, and Watt energy spectra. The Watt energy spectrum was chosen for this project. It accounts for prompt fission neutrons with a continuous energy spectrum. The most probable energy of this spectrum occurs at 0.73 MeV (Lamarsh, 1983).

Approximately 99% of the neutrons released during fission are prompt neutrons (Lamarsh, 1983).

In MCNP the Watt fission spectrum is calculated with the following equation:

$$f(E) = Ce^{-(E/a)} \cdot \sinh(bE)^{1/2} \quad \text{(Equation 9) (Briesmseister, 2000)}$$

When modeling neutron induced fission in HEU, $a = 0.988$ MeV and $b = 2.249$ MeV.

For weapons grade plutonium, $a = 0.966$ MeV and $b = 2.842$ MeV (Briesmseister, 2000).

C serves as a normalizing constant for the program since the output for the particle

history is normalized to one particle. The Watt energy distribution function was first tested and compared to the theoretical output described in Equation 9 (Figure 4).

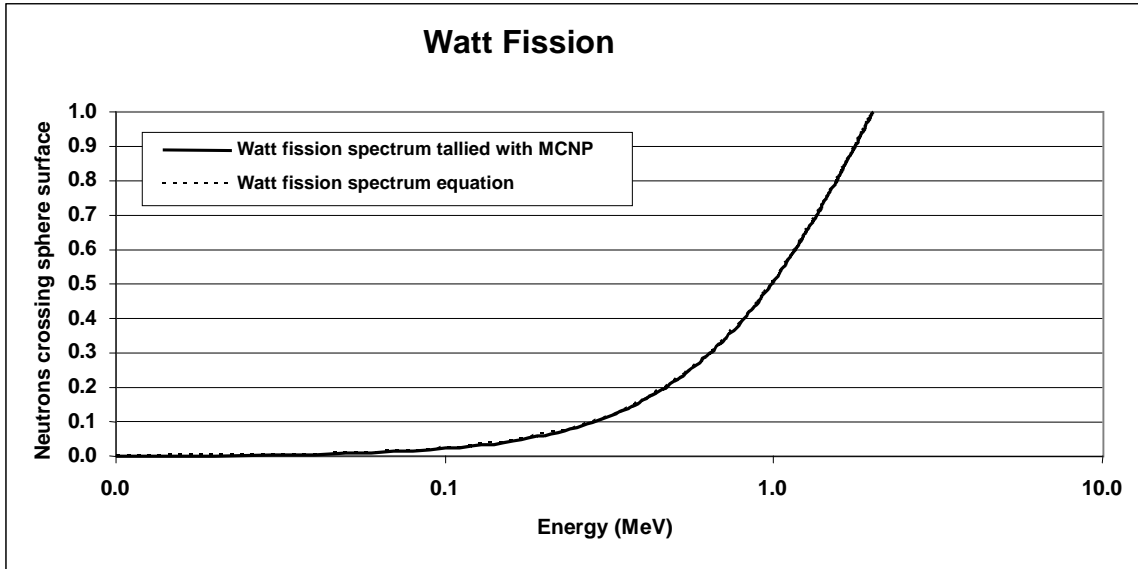


Figure 4. Cumulative distribution of the theoretical Watt fission spectrum vs. the Watt fission spectrum calculated with MCNP.

Once the Watt fission spectrum was verified as correct the computer code input was then tested among sources of differing geometries. Three basic source geometries were modeled: a sphere, a cylinder, and a sheet. Each weighed 500g and had a uniform distribution of HEU throughout the volume. The tally was recorded at the surface of a 200 cm radius sphere (Figure 5).

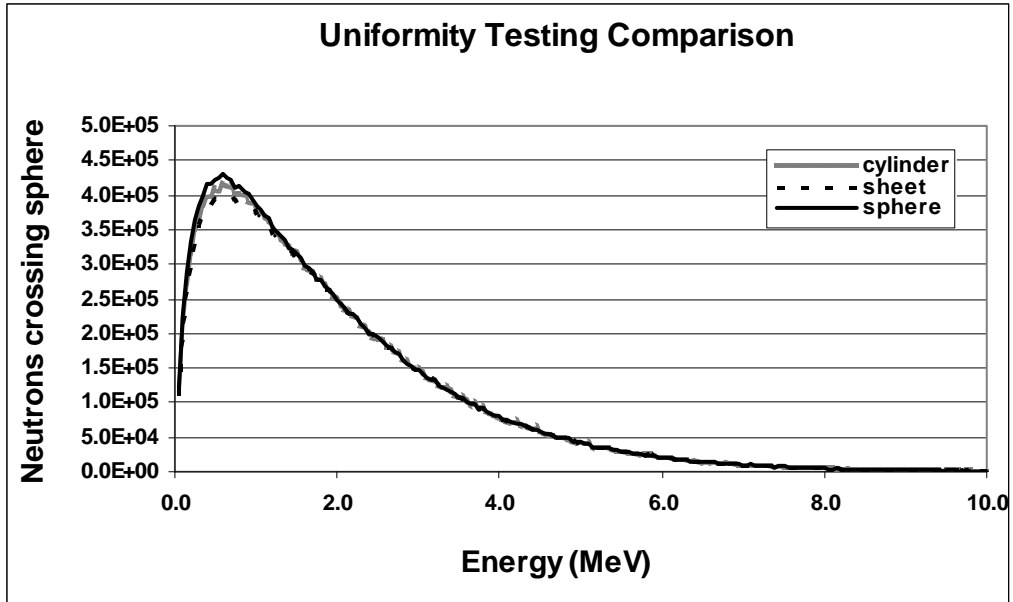


Figure 5. Output of the source geometry modeling. Each source consisted of HEU, uniformly distributed throughout the source volume. The sources each weighed 500g. 20,000,000 neutrons were tracked for each source and the tally was recorded at the surface of a 200 cm radius sphere surrounding the source.

RESULTS AND DISCUSSION

When the basic MCNP functions were verified as input correctly, the modeling of spectra emitted from different configurations was started. This process began by adding six 50 cm x 50 cm x 1 cm detectors to each configuration. Detector surfaces were placed on six different sides so that they were exactly opposite each other as shown in Figures 6, 7, and 8. Tallies were scored at 100 cm from the isocenter of the source on each detector and at the surface of a 200 cm sphere surrounding the source. No material was placed outside of the detector surfaces, therefore, the neutrons traversed a void space once they left the source. This void space was essentially a vacuum. The only modifying factor for these runs was the shape of the source. Each source weighed 500 g for each source and had a density of 18.7 g/cm^3 .

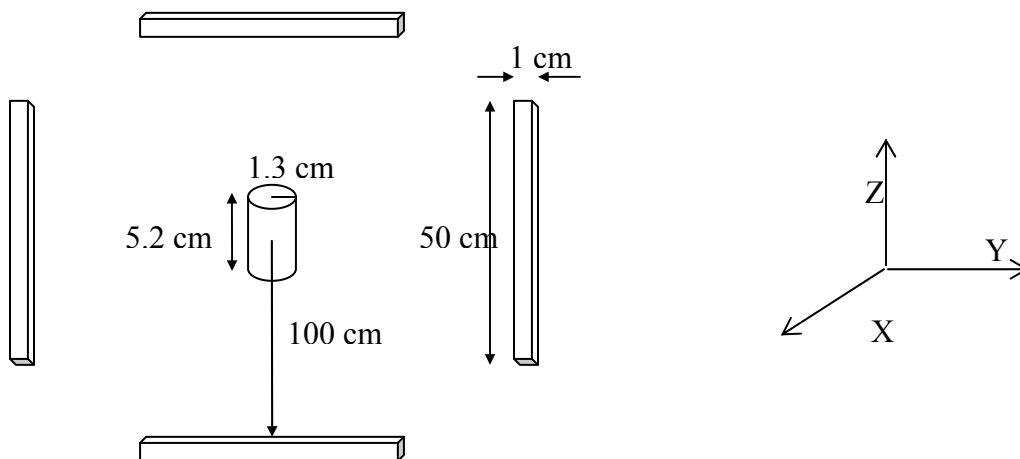


Figure 6. Configuration of a uniform cylinder source consisting of 500g of HEU, radius = 1.3 cm, height = 5.2 cm density = 18.7 g/cm^3 , surrounded by six detector surfaces. Each detector surface is 100 cm from the center of the cylinder and has dimensions of 50 x 50 x 1 cm.

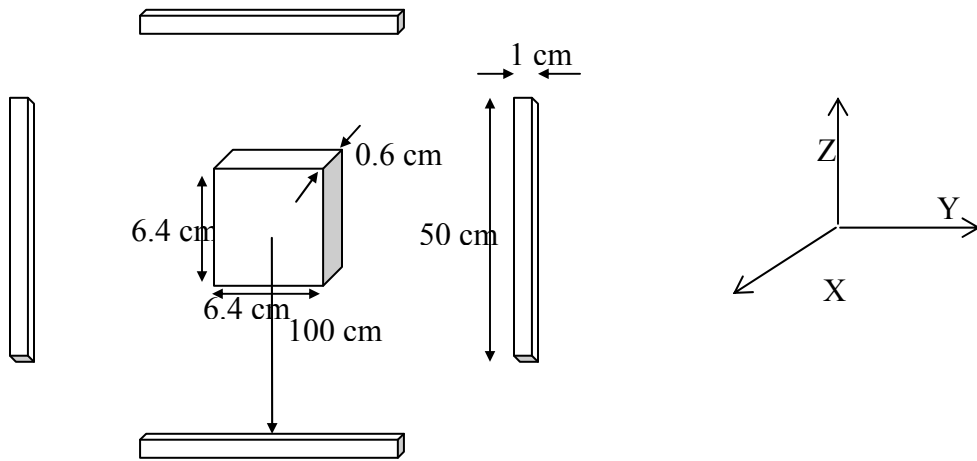


Figure 7. Configuration of a uniform sheet source consisting of 500g of HEU, depth = 0.6 cm, height = 6.4 cm, density = 18.7 g/cm³, surrounded by six detector surfaces. Each detector surface is 100 cm from the center of the cylinder and has dimensions of 50 x 50 x 1 cm.

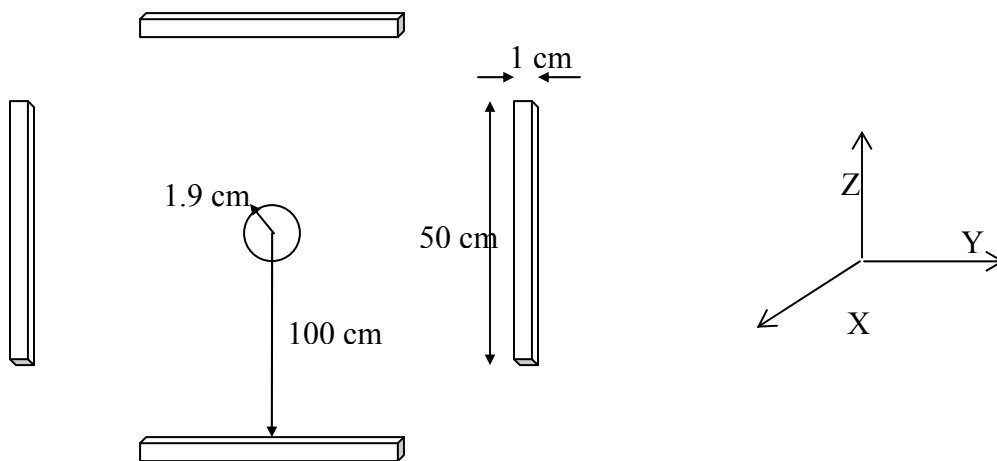


Figure 8. Configuration of a uniform sphere source consisting of 500g of HEU, radius = 1.9 cm, density of 18.7 g/cm³, surrounded by six detector surfaces. Each detector surface is 100 cm from the center of the cylinder and has dimensions of 50 x 50 x 1 cm.

The configurations shown in figures 6, 7, and 8 were calculated over an energy range of 1×10^{-6} – 10 MeV. The resulting neutron current data were then compared to one another at the surface of the 200 cm empty sphere surrounding each source. These configurations were also compared to the neutron spectrum emitted from a point source with a basic Watt distribution (Figure 9). The cumulative distribution was calculated for

each different configuration. The cumulative distribution is compared at the 100 KeV point. The relative error of the tally is displayed in Table C-1.

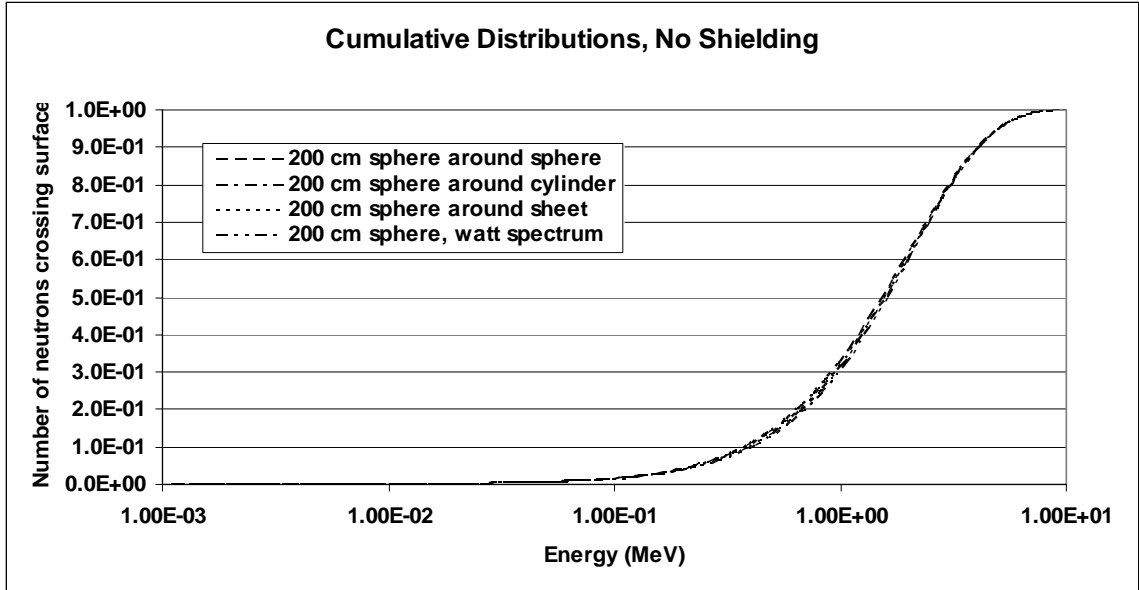


Figure 9. Cumulative distribution of neutron current at 200 cm empty sphere surface for basic source configurations with no shielding. The cylinder, sheet, and sphere each represent a 500 g HEU source with a uniform distribution. The Watt spectrum was run as a point source.

Figure 9 indicates that there was no significant difference of energy distributions.

Table 1 shows the numerical value of the percent neutrons crossing the surrounding sphere surface at energies below 1.0×10^{-3} %. The largest difference between the various configurations is 2.3×10^{-6} %. This is an extremely small difference. There is no significant change in the shape of the curve from source to source. This indicates that self-absorption within the source volume is not significant enough to alter the shape of the various neutron spectra.

Table 1. Comparison of cumulative distributions. The percentage of neutrons crossing the surface of the 200 cm sphere is shown for neutrons with energies of less than 1.0×10^{-3} MeV for a 500 g cylinder, sheet, and sphere without shielding, and a point source with a Watt distribution.

Comparison of Cumulative Distributions (%)				
Energy (MeV)	Cylinder no shielding	Sheet no shielding	Sphere no shielding	Watt spectrum
$<1.0 \times 10^{-3}$	1.17×10^{-3}	1.34×10^{-3}	1.13×10^{-3}	1.36×10^{-3}

Table 1 shows that the majority of the neutrons emitted from each source volume cross the 200 cm empty sphere surface at an energy which is greater than 1×10^{-3} MeV. This is to be expected as there is no moderating material between the source volume and the sphere surface. It can be seen from Table C-1 that as the energy bins fall below 1×10^{-5} MeV, the relative error becomes significantly larger. In this region it is difficult to achieve good statistics because of the lack of neutron moderation. A detector trying to count neutrons from an unshielded source in this region will not yield reliable data unless moderating material is placed around the detector volume.

The sphere volume was then surrounded with a series of polyethylene spheres concentric with the source volume. The spheres were placed at intervals with radii equal to 5 cm, 10 cm, 15 cm, and 20 cm from the center of the source volume as shown in Figure 10.

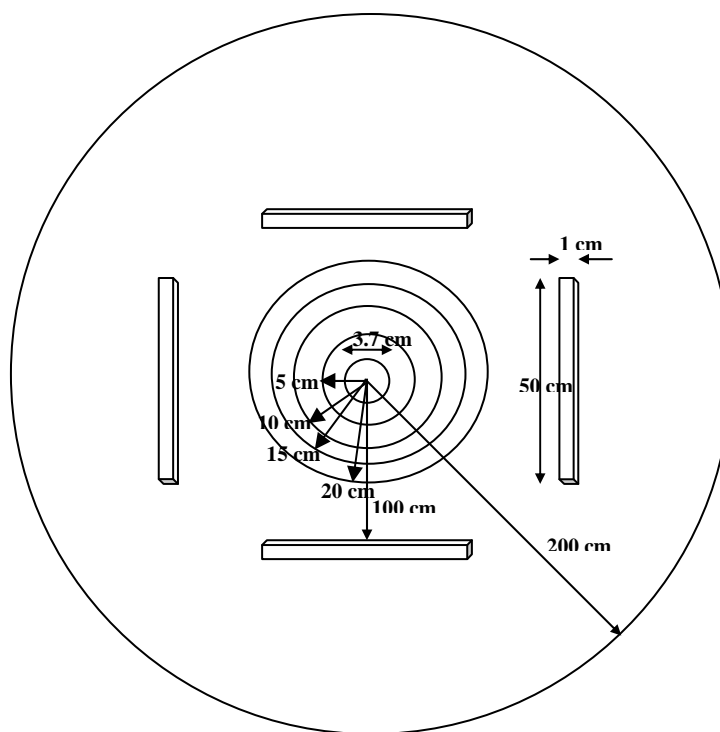


Figure 10. Uniform sphere of 500 g of HEU with a radius of 1.9 cm surrounded by polyethylene spheres concentric on the source volume. The surrounding polyethylene spheres have radii of 5 cm, 10 cm, 15 cm, and 20 cm. An empty sphere with a 200 cm radius surrounds the configuration. Neutron current tallies for this configuration were collected at the surface of the 200 cm sphere.

Figure 10 indicates that for this configuration, there is an optimal thickness for neutron moderation. Above that thickness, neutrons will be attenuated instead of moderated. This will be important to consider when designing a detector if polyethylene is used as a moderator around the detector volume. For the unshielded sphere source at energies below 1×10^{-3} MeV, the relative error increases as the energy decreases due to the lack of neutron moderation (Table C-2). For the tallies recorded with polyethylene surrounding the source volume, the relative error becomes insignificant (Table C-2). This indicates that any amount of moderating material added to the source-detector

configuration will improve the statistics for the number of neutrons crossing at lower energies.

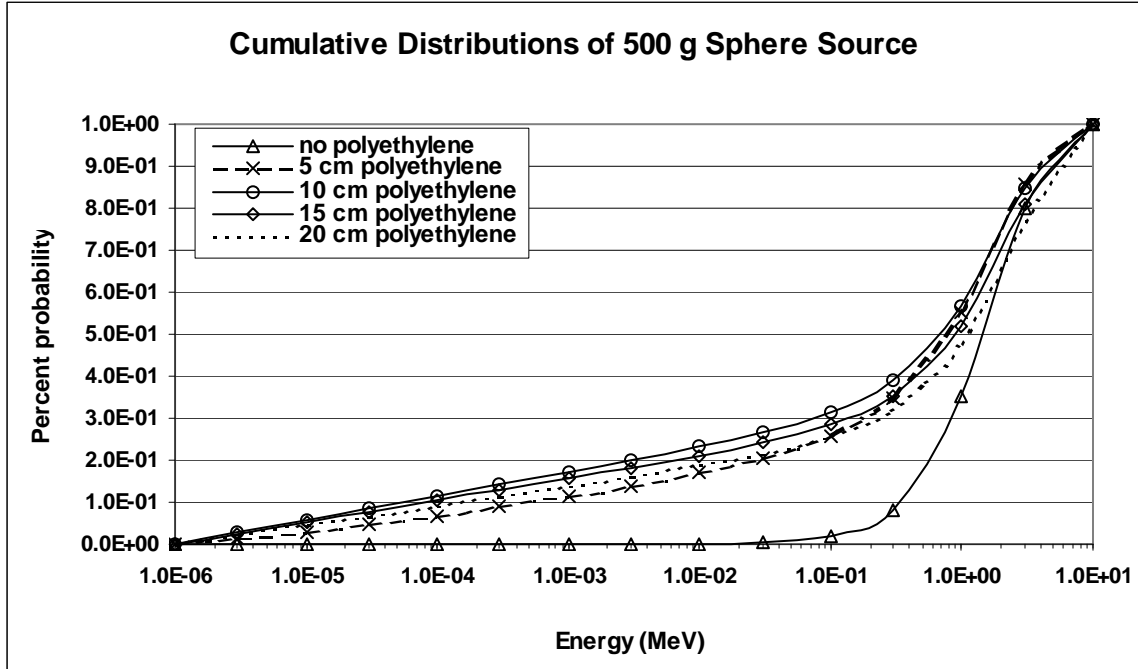


Figure 11. The cumulative distributions of a 500 g sphere of HEU is surrounded by no shielding, 5 cm of polyethylene, 10 cm of polyethylene, 15 cm of polyethylene, and 20 cm of polyethylene. The neutron current tallies are recorded along the 200 cm empty sphere surface.

Table 2 displays the percent neutrons crossing the 200 cm surrounding sphere surface at an energy of less than or equal to 1.0×10^{-3} MeV. As the thickness of polyethylene increases above 10 cm, the percent neutrons crossing below 1.0×10^{-3} MeV decreases. For neutrons emitted from weapons grade nuclear material, polyethylene will start to become a shielding material as opposed to a moderating material at thicknesses of greater than 10 cm. This is more pronounced as the energy increases. A point was also compared for neutrons crossing the surface at less than or equal to 3.0×10^{-1} MeV, demonstrating this pattern (Table 2).

Table 2. Comparison of cumulative distributions. The percentage of neutrons crossing the surface of the 200 cm sphere is shown for neutrons with energies of less than 1.0×10^{-3} MeV for a 500 g sphere of uniformly distributed HEU without shielding, 5 cm of polyethylene, 10 cm of polyethylene, 15 cm of polyethylene, and 20 cm of polyethylene. The data is again compared for neutrons crossing the sphere surface at or below 3.0×10^{-1} MeV.

Comparison of Cumulative Distributions (%)					
Energy (MeV)	Sphere, no poly-ethylene	5 cm poly-ethylene	10 cm poly-ethylene	15 cm poly-ethylene	20 cm poly-ethylene
$<1.0 \times 10^{-3}$	1.17×10^{-3}	11.4	17.2	15.6	13.9
$<3.0 \times 10^{-1}$	8.3	34.7	39.0	35.4	32.1

Throughout the remainder of the research, only cylinder and sheet sources are modeled in MCNP since a literature review revealed that these were the most likely geometries in which a source would be smuggled (IAEA, 2003). It would be difficult to smuggle HEU or ^{239}Pu in the shape of a sphere, as this is the best volume to achieve criticality, thereby making transport of the material an extremely difficult challenge.

The next configurations tested with MCNP consisted of the same configurations with a different source weight. The weight of each uniform source was increased to 2000 g of HEU. The density remained the same but the volumes were altered. The ratio of dimensions was kept the same for the increased volumes. The cylinder remained at 2:1 ratio for height versus radius, and the sheet remained at a ratio of 10:10:1 for height versus width versus depth. The cumulative distribution comparisons can be seen in Figure 12.

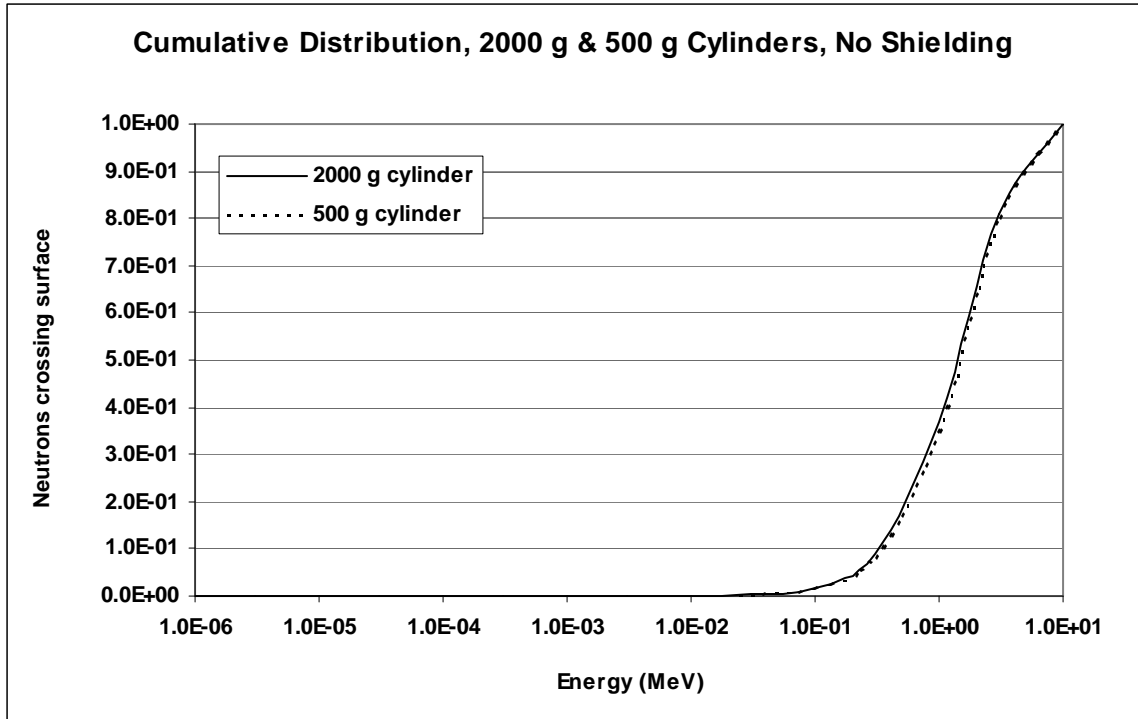


Figure 12. Cumulative distribution for the number of neutrons crossing the surface of an empty sphere with a radius of 200 cm. One cylinder contains 500 g of HEU with a uniform distribution. The other cylinder contains 2000 g of HEU with a uniform distribution.

There was no significant difference in the cumulative distribution based on the change in weight of the cylinder source. The difference between the fraction of neutrons crossing the sphere surface at less than or equal to 1.0×10^{-3} MeV for the two different volumes is $1.2 \times 10^{-4}\%$ (Table 3). This indicates that there is no significant change in the shape of the curve of the cumulative distribution for the different sources.

Table 3. Comparison of cumulative distributions. The percentage of neutrons crossing the surface of the 200 cm sphere is shown for neutrons with energies of less than 1.0×10^{-3} MeV for a 500 g cylinder and a 2000 g cylinder of uniformly distributed HEU without shielding.

Comparison Point for Cumulative Distribution (%)		
Energy (MeV)	Cylinder (500 g)	Cylinder (2000 g)
$<1.0 \times 10^{-3}$	1.17×10^{-3}	1.05×10^{-3}

The sheet source is also compared in Figure 13. Although the volume of the HEU source is increased by a factor of four, very little difference exists between the cumulative distributions.

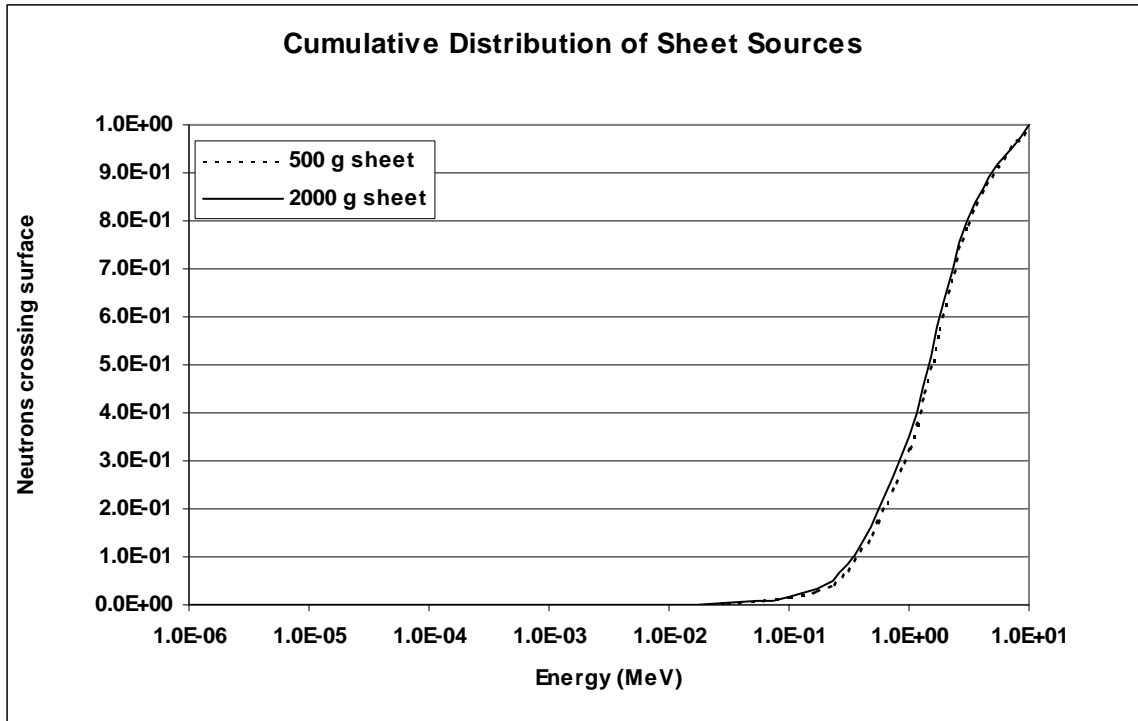


Figure 13. The cumulative distribution for the neutron current crossing the surface of a surrounding empty sphere at a 200 cm radius. One sheet represents a 500 g HEU source with a uniform distribution. The other sheet represents a 2000 g HEU source with a uniform distribution.

The cumulative distributions of the sheet sources are quantitatively compared in Table 4. The difference in the percent distribution for the number of neutrons crossing the surface of an empty surrounding sphere at 200 cm for the two configurations is $8.0 \times 10^{-5}\%$. This indicates that there is no significant difference between the cumulative distributions from a 500 g sheet to a 2000 g sheet. The relative error of the tally results are noted in Table C-3.

Table 4. Comparison of cumulative distributions. The percentage of neutrons crossing the surface of the 200 cm sphere is shown for neutrons with energies of less than 1.0×10^{-3} MeV for a 500 g sheet and a 2000 g sheet of uniformly distributed HEU without shielding.

Comparison of Cumulative Distributions (%)		
Energy (MeV)	Sheet (500 g)	Sheet (2000 g)
$<1.0 \times 10^{-3}$	1.30×10^{-3}	1.22×10^{-3}

The neutron current crossing the detector surfaces was then compared among the different axes for the 500 g cylinder source (Figures 14). The configuration is the same as that in Figure 6. The tallies are recorded at the surface of flat detector surfaces placed 100 cm away from the center of the source volume.

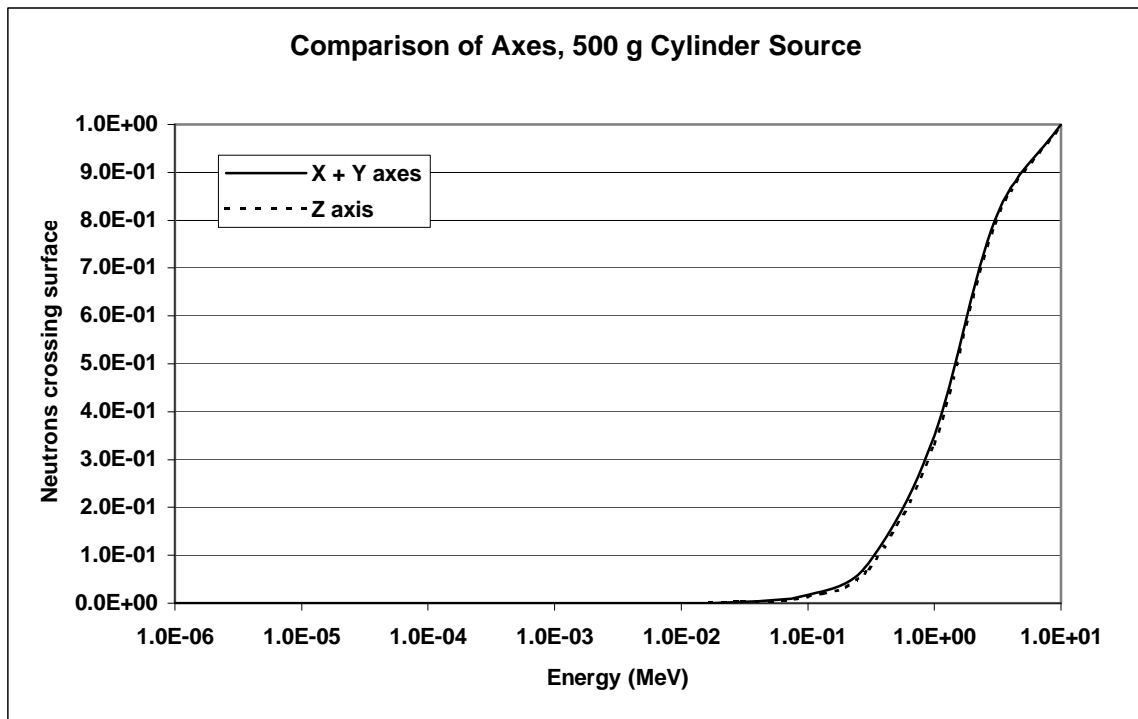


Figure 14. The cumulative distribution for the number of neutrons crossing a flat detector surface of 2500 cm^2 at a distance of 100 cm from the center of the source. The neutrons originate from a 500 g cylinder source of uniformly distributed HEU. The neutron currents were averaged for the two detectors which fall along each axis. The X and Y axes data is averaged and normalized to one.

The cumulative distribution of the neutron current for X + Y axes was compared to the cumulative distribution of the neutron current for the Z axis for neutrons crossing the detector surfaces at 1.0×10^{-3} MeV and below (Table 5). This indicates that the cumulative distributions of the neutron current are the same for all of the detectors surrounding an unshielded cylinder source. Percent probability of a neutron crossing at 1.0×10^{-3} MeV and below is displayed in Table 5. The difference of these distributions is 2.8×10^{-4} MeV.

Table 5. Comparison of cumulative distributions. The percentage of neutrons crossing the surface of the 200 cm sphere is shown for neutrons with energies of less than 1.0×10^{-3} MeV for a 500 g cylinder of uniformly distributed HEU without shielding. The neutron currents were averaged for the two detectors which fall along each axis. The X and Y axes data is averaged and normalized to one.

Comparison Point for Cumulative Distribution (%)		
Energy (MeV)	Cylinder X + Y axes	Cylinder Z axis
$<1.0 \times 10^{-3}$	1.2×10^{-3}	9.2×10^{-4}

Table C-3 indicates the relative error pertaining to each detector surface. The relative error begins to decrease rapidly at neutron energies above 3.0×10^{-4} MeV. Although relative error of the neutron current tallies below 3.0×10^{-4} MeV is high, the data is still useful as it gives an indication of how neutrons in this energy region will track. The data along the Z axis shows a slightly higher relative error than the other axes. This occurs because the cylinder is oriented so that the base of the cylinder lies along the Z axis as shown in Figure 6. Since the base of the cylinder has a smaller surface area than the side of the cylinder, the particle statistics emitted from this surface will be slightly degraded.

The tally recorded for the sheet source with no shielding material gave results similar to the basic cylinder tallies (Figure 15).

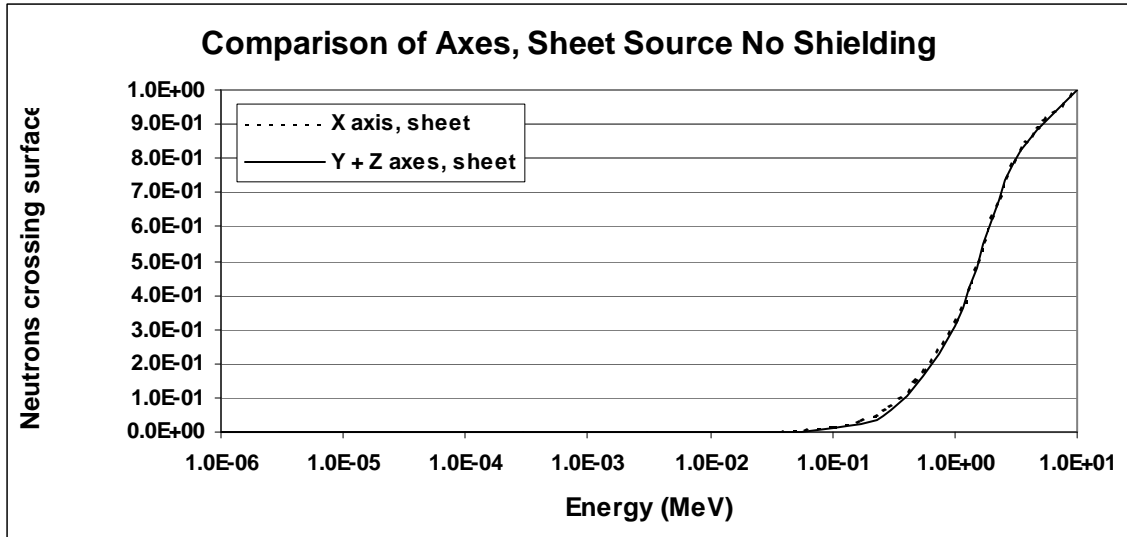


Figure 15. The cumulative distribution for the number of neutrons crossing a flat detector surface of 2500 cm² at a distance of 100 cm from the center of the source. The neutrons originate from a 500 g sheet source of uniformly distributed HEU. The neutron currents were averaged for the two detectors which fall along each axis. The Y and Z axes data is averaged and normalized to one.

The surface area for the source along the Y and Z axes are the same, so these axes are normalized into one axis for simplicity. No significant difference can be seen among the axes. The relative error of the neutron current as calculated by MCNP is shown in Table C-4. The X axis indicates slightly better statistics than the Y and Z axes. This is because the surface area of the source along the X axis is significantly larger than the surface areas along the Y and Z axes. There appears to be no significant change in the cumulative distribution curve for the X axis versus the Y + Z axes. This is quantitatively compared in Table 6.

Table 6. Comparison of cumulative distributions. The percentage of neutrons crossing the surface of the 200 cm sphere is shown for neutrons with energies of less than 1.0×10^{-3} MeV for a 500 g sheet of uniformly distributed HEU without shielding. The neutron currents were averaged for the two detectors which fall along each axis. The Y and Z axes data is averaged and normalized to one.

Comparison Point for Cumulative Distribution (%)		
Energy (MeV)	Sheet Y+Z axes	Sheet X axis
$<1.0 \times 10^{-3}$	9.8×10^{-4}	1.7×10^{-3}

The difference between the percent of neutrons crossing the various detector surfaces at or below 1.0×10^{-3} MeV is approximately 7.2×10^{-3} %. Although this difference is small, there appears to be a slightly higher volume of neutrons crossing the detector surfaces along the X axis as opposed to the Y + Z axes. This likely occurs because the surface area of the source along the X axis is 10 times larger than the surface areas along the other axes.

Dry air (Appendix B) was then added to the configurations. It resulted in no significant impact on the neutron tally. Polyethylene (Appendix B) was also added to each configuration. This material was modeled in such a way as to represent a shielding configuration that could fit into a small suitcase. The first configuration consisted of a 500 g cylinder of uniformly distributed HEU. The cylinder was surrounded by a block of polyethylene with dimensions of 7.5 x 20 x 15cm (Figure 16). This sort of configuration equates to only 5 pounds of material.

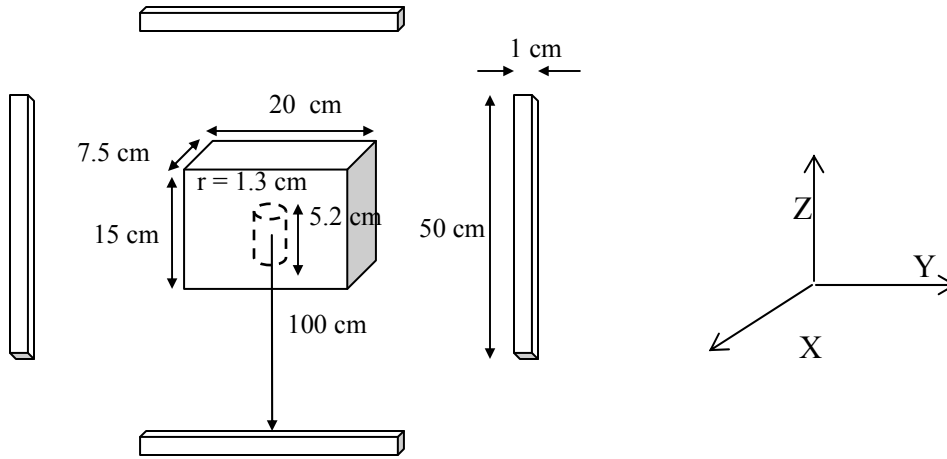


Figure 16. This configuration demonstrates a uniform source of HEU in the shape of a cylinder, density = 18.7 g/cm^3 , surrounded by a $7.5 \times 20 \times 15$ cm block of polyethylene with a density of 0.94 g/cm^3 . The polyethylene and HEU cylinder are surrounded on six sides by $50 \times 50 \times 1$ cm detector surfaces.

The tally data from the model described in Figure 16 shows a slight vertical shift of the cumulative distribution for neutron current along the X axis over the Y and Z axes (Figure 17). The difference of cumulative distributions does not appear to be as pronounced between the Y and Z axes. This occurs because of the combination of thin shielding material along the X axis and the ideal surface area of the source in the X axis orientation. The point along this axis with the least amount of shielding consists of 0.75 cm of polyethylene between the source volume and the detector surface. Polyethylene contains 1.4% Hydrogen (Appendix B). The cross section of Hydrogen makes it the most efficient element for moderating thermal neutrons (Appendix A). Since more Hydrogen is placed between the source volume and the detector surface along the Z axis than along the X axis, the expected result would be that fewer neutrons would be moderated along the X axis.

In the Y direction, the shielding between the source volume and the detector is the thickest. The thickness of the polyethylene shielding in this orientation is 7 cm. The

increased shielding thickness along with the surface area advantage combine to give a neutron current similar to that of crossing the Z axis detectors.

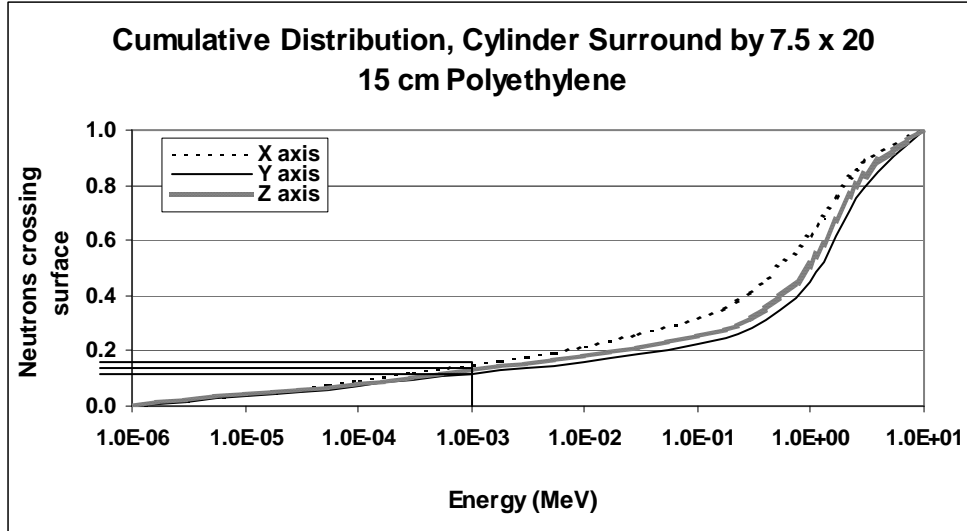


Figure 17. The cumulative distribution for the number of neutrons crossing a flat detector surface of 2500 cm² at a distance of 100 cm from the center of the source along the X, Y and Z axes. The neutrons originate from a 500 g cylinder source of uniformly distributed HEU. The source is surrounded by polyethylene with dimensions of 7.5 x 20 x 15 cm. All data is normalized to 1 neutron particle.

This indicates that the cumulative distribution of the neutron current along the X axis is slightly different than that along the Y and Z axes. The percent distribution of neutrons crossing the detector surface at and below 100 KeV is highest along the X axis and lowest along the Z axis (Table 7). The distributions below this energy point vary by 3.8%.

Table 7. Comparison of cumulative distributions. The percentage of neutrons crossing flat detector surfaces of 2500 cm² at a distance of 100 cm from the center of the source along the X, Y and Z axes at energies of less than 1.0 x 10⁻³ MeV. The source volume is a 500 g cylinder of uniformly distributed HEU surrounded by polyethylene with dimensions of 7.5 x 20 x 15 cm.

Comparison of Cumulative Distributions (%)			
Energy (MeV)	X axis	Y axis	Z axis
1.0 x 10 ⁻³	15.3	11.5	12.9

The statistics of the neutron current tally scored by MCNP for the 500 g cylinder surrounded by 7.5 x 20 x 15 cm of polyethylene are displayed in Table C-5. It should be noted that the statistics for the neutron tallies at 1.0×10^{-3} MeV and below improve dramatically when moderating material is added. This occurs because of the increased number of neutrons crossing at the lower energy ranges.

The thickness of the shielding material was then modified as shown in Figure 18, and the neutron tally was computed with MCNP. The polyethylene was oriented somewhat differently around the cylinder. This was done to demonstrate the affect of a different orientation and thickness of the shielding material around an HEU source as it is difficult to guess exactly what type of material would be used to shield concealed weapons grade material.

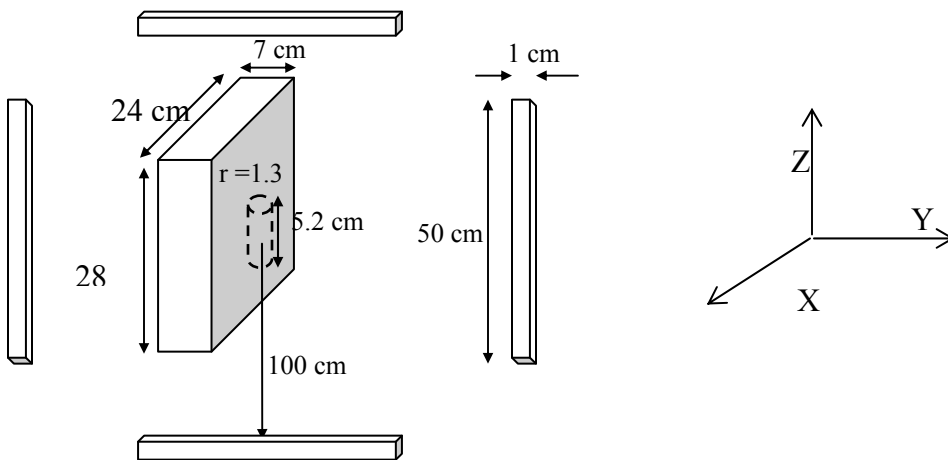


Figure 18. This configuration demonstrates a uniform source of HEU in the shape of a cylinder, density = 18.7 g/cm^3 , surrounded by a $24 \times 7 \times 28 \text{ cm}$ block of polyethylene with a density of 0.94 g/cm^3 . The polyethylene and HEU cylinder are surrounded on six sides by $50 \times 50 \times 1 \text{ cm}$ detector surfaces.

The cumulative distribution of the neutron current was compared among the detector surfaces along the different axes (Figure 19).

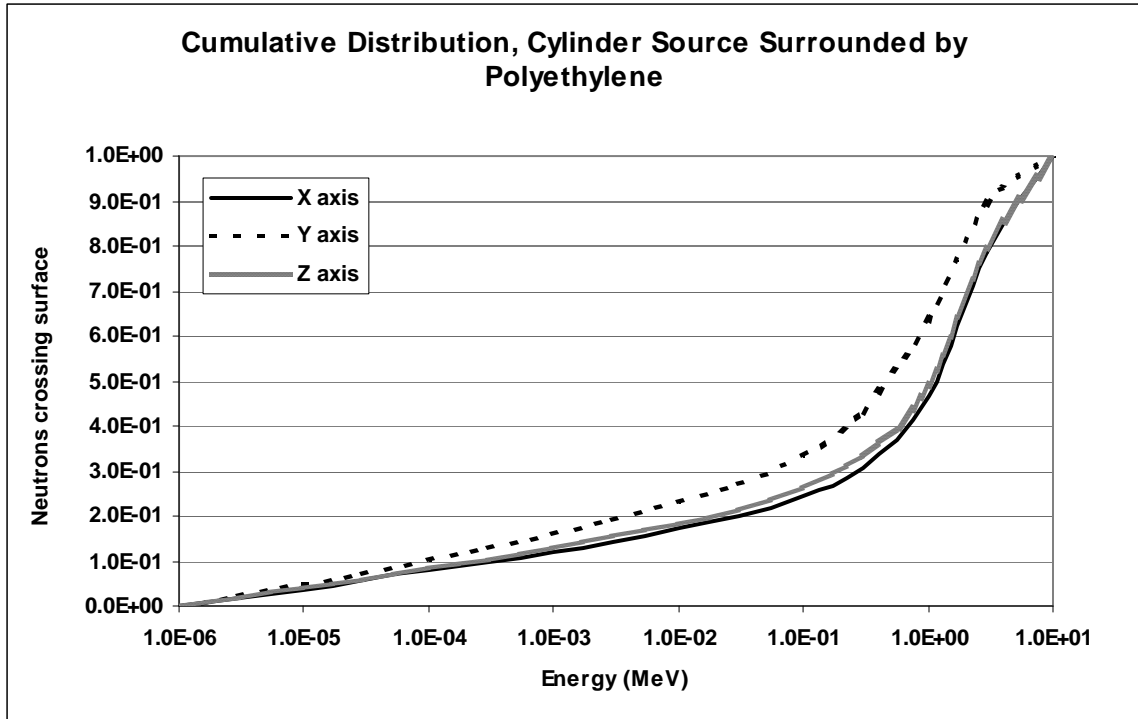


Figure 19. The cumulative distribution for the number of neutrons crossing a flat detector surface of 2500 cm² at a distance of 100 cm from the center of the source along the X, Y and Z axes. The neutrons originate from a 500 g cylinder source of uniformly distributed HEU. The source is surrounded by polyethylene with dimensions of 24 x 7 x 28 cm. All data is normalized to 1 neutron particle.

It appears as though the current distribution along the Y and Z axis is the same but that the current along the X axis has shifted. The detector along the X axis for the 7.5 x 20 x 15 cm polyethylene configuration shows that fewer neutrons are crossing the detector surface at or below 1.0×10^{-3} MeV. This is to be expected as this orientation provides the least amount of moderating material. The quantitative differences between the cumulative distributions for the three axes are displayed in Table 8. The relative error of for the neutron current along the various axes is shown in Table C-6.

Table 8. Comparison of cumulative distributions. The percentage of neutrons crossing flat detector surfaces of 2500 cm² at a distance of 100 cm from the center of the source along the X, Y and Z axes at energies of less than 1.0 x 10⁻³ MeV. The source volume is a 500 g cylinder of uniformly distributed HEU surrounded by polyethylene with dimensions of 24 x 7 x 28 cm polyethylene shielding.

Comparison of Cumulative Distributions (%)			
Energy (MeV)	X axis	Y axis	Z axis
1.0 x 10 ⁻³	12.2	16.0	12.9

The neutron current is then compared for the different polyethylene thicknesses along the X axis (Figure 20).

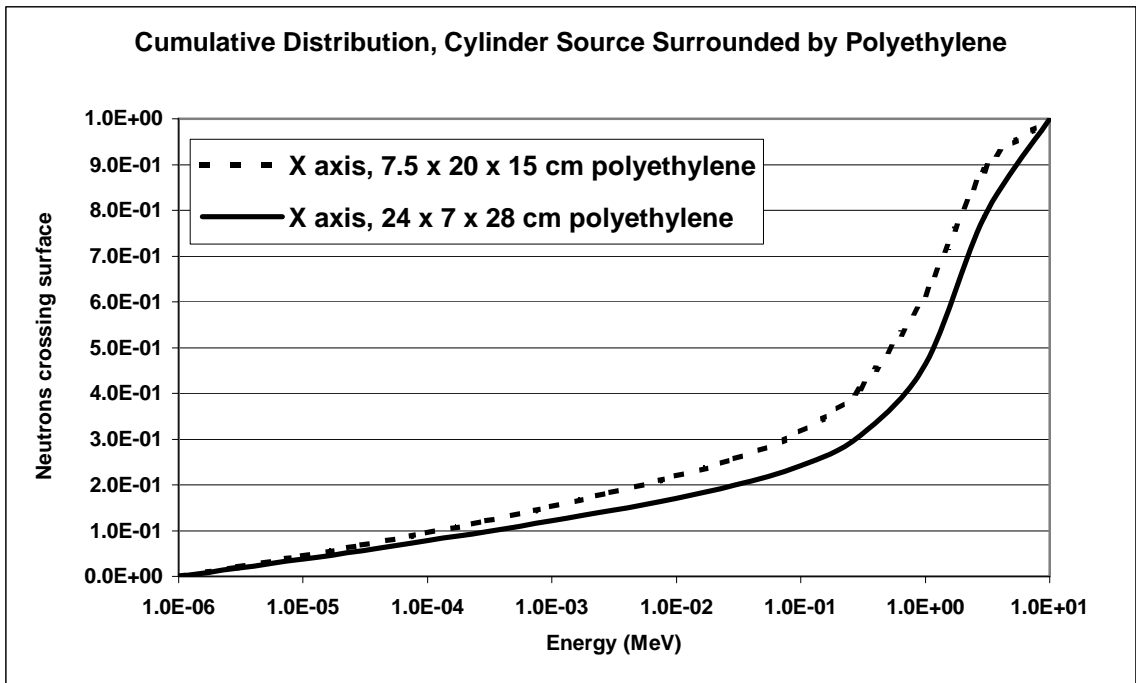


Figure 20. Tally of neutrons crossing the detector surfaces along the X axis for the 500 g HEU cylinder surrounded by polyethylene with dimensions of 7.5 x 20 x 15 cm. This is compared to the same cylinder volume surrounded by 24 x 7 x 28 cm of polyethylene. All data is normalized to 1 neutron particle.

The percent probability of the cumulative distribution along the X axis for neutrons crossing the detector surface at or below 1.0 x 10⁻³ MeV is compared for the different configurations in Table 9.

Table 9. Comparison of cumulative distributions. The percentage of neutrons crossing flat detector surfaces of 2500 cm² at a distance of 100 cm from the center of the source along the X axis at energies of less than 1.0 x 10⁻³ MeV. The source volumes are a 500 g cylinder of uniformly distributed HEU surrounded by polyethylene with dimensions of 7.5 x 20 x 15 cm of polyethylene shielding and 24 x 7 x 28 cm polyethylene shielding.

Comparison Point for Cumulative Distribution (%)		
Energy (MeV)	X axis 7.5 x 20 x 15 cm polyethylene shielding	X axis 24 x 7 x 28 cm polyethylene shielding
<1.0 x 10 ⁻³	9.8 x 10 ⁻⁴	1.7 x 10 ⁻³

Polyethylene material was then placed around a uniform sheet source of 500 g of HEU. The source volume had the same dimensions as the volume tested for the configuration shown in Figure 7. The polyethylene was given dimensions of 7.5 x 20 x 15 cm. These were consistent with the shielding material placed around the cylinder as shown in Figure 17. The resulting configuration is displayed in Figure 21.

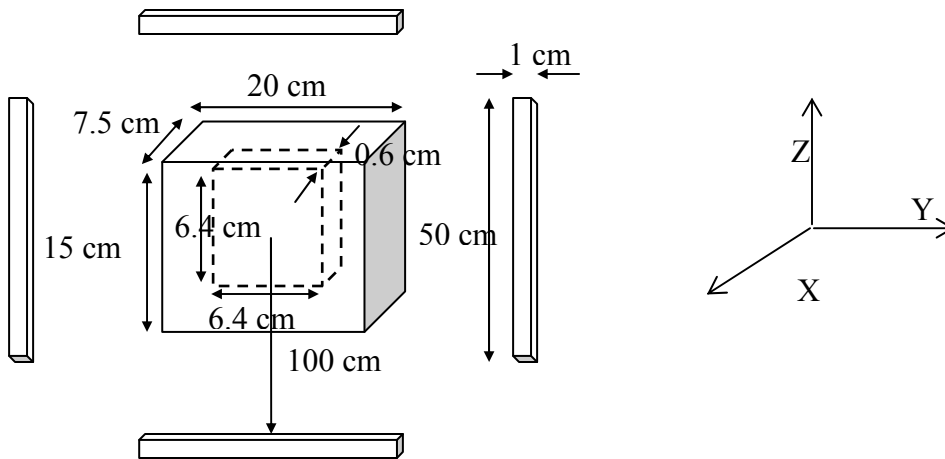


Figure 21. This configuration demonstrates a uniform source of HEU in the shape of a sheet surrounded by a 7.5 x 20 x 15 cm block of polyethylene with a density of 0.94 g/cm³. The polyethylene and HEU sheet are surrounded on six sides by 50 x 50 x 1 cm detector surfaces.

The resulting output is displayed in Figure 22. It should be noted that the neutron current for energies above 1.0 x 10⁻³ MeV along the X axis is higher than the current

along the Z axis. This occurs because of the combination of the source geometry and the shielding thickness. The surface area along the X axis is 10 times larger than the surface area along the Z axis. The shielding material along the Z axis is 0.9 cm thicker than the shielding along the X axis.

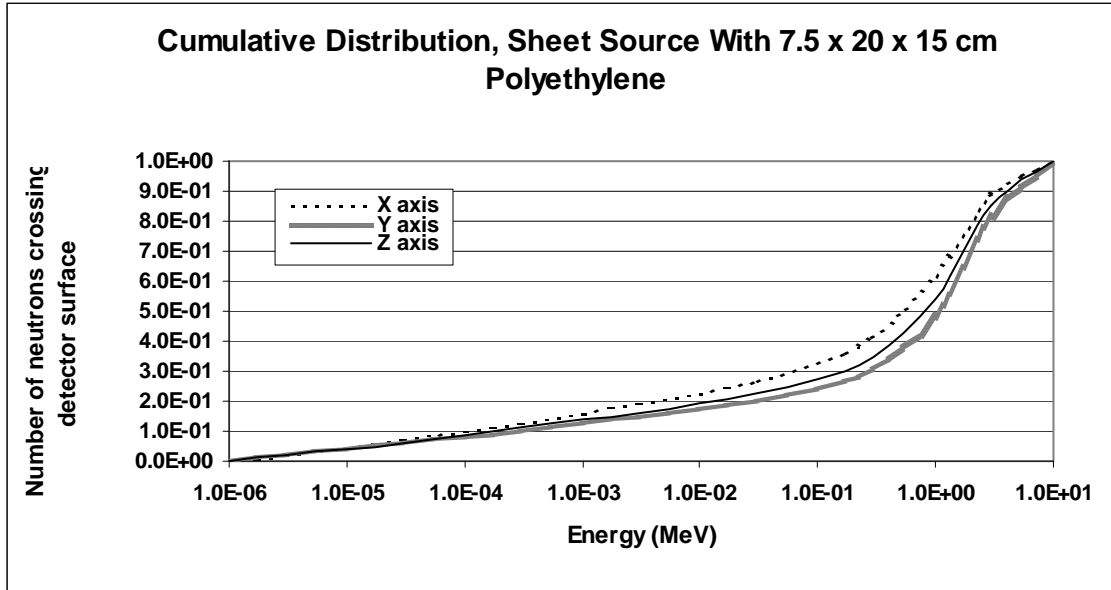


Figure 22. The cumulative distribution for the number of neutrons crossing a flat detector surface of 2500 cm² at a distance of 100 cm from the center of the source along the X, Y and Z axes. The neutrons originate from a 500 g sheet source of uniformly distributed HEU. The source is surrounded by polyethylene with dimensions of 7.5 x 20 x 15 cm. All data is normalized to 1 neutron particle.

The cumulative distribution below the 1.0×10^{-3} MeV mark appears to be very similar along the three axes. This is quantitatively compared in Table 10. The cumulative distribution is also compared at the 1.0×10^{-1} MeV mark to show the divergence of distributions between the axes as the energies increase for this configuration. The difference between the cumulative distributions at the for the X and Y axes increases from 3.5% at energies below 1.0×10^{-3} MeV to 8.2% at energies below 1.0×10^{-1} MeV. The relative error for this data can be found in Table C-7.

Table 10. Comparison of cumulative distributions. The percentage of neutrons crossing flat detector surfaces of 2500 cm² at a distance of 100 cm from the center of the source along the X, Y and Z axes at energies of less than 1.0 x 10⁻³ MeV and again at energies of 1.0 x 10⁻¹ MeV or lower. The source volumes are a 500 g sheet of uniformly distributed HEU surrounded by polyethylene with dimensions of 7.5 x 20 x 15 cm of polyethylene shielding.

Comparison Point for Cumulative Distribution (%)			
Energy (MeV)	X axis	Y axis	Z axis
1.0 x 10 ⁻³	16.1	12.6	13.7
1.0 x 10 ⁻¹	32.4	24.2	27.2

The statistics for this configuration are provided in Table C-7. The statistics for the neutron tallies crossing the detectors along the X axis are slightly better than the statistics for the detectors along the Z axis. This happens because the larger the surface area of the source volume, the greater number of neutrons will be emitted. As the neutron current increases the statistics will likewise improve.

The configuration was then modified by changing the thickness of the polyethylene material to dimensions of 24 x 12 x 28 cm (Figure 23).

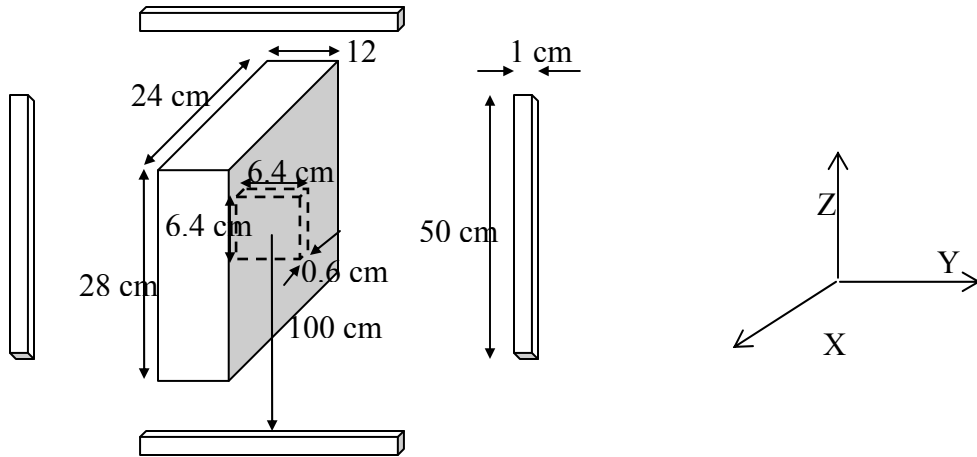


Figure 23. This configuration demonstrates a uniform source of HEU in the shape of a sheet weighing 500 g surrounded by a 24 x 12 x 28 cm block of polyethylene with a density of 0.94 g/cm³. The polyethylene and HEU cylinder are surrounded on six sides by 50 x 50 x 1 cm detector surfaces.

The neutron current along the X, Y and Z axes was then compared (Figure 24).

The shielding along the X axis is 11.7 cm thick on either side of the HEU sheet. The shielding along the Y axis is 2.8 cm thick on either side of the HEU sheet, and the shielding along the Z axis is 7 cm thick on either side of the HEU sheet. The greatest difference between shielding thickness exists between the X and Y axes. Although there is a greater amount of polyethylene along the X axis, the surface area of the source volume along this axis is larger. In this configuration, the differences in the cumulative distribution of the neutron current crossing the detector surfaces is likely driven more by moderator thickness than by the surface area of the source volume.

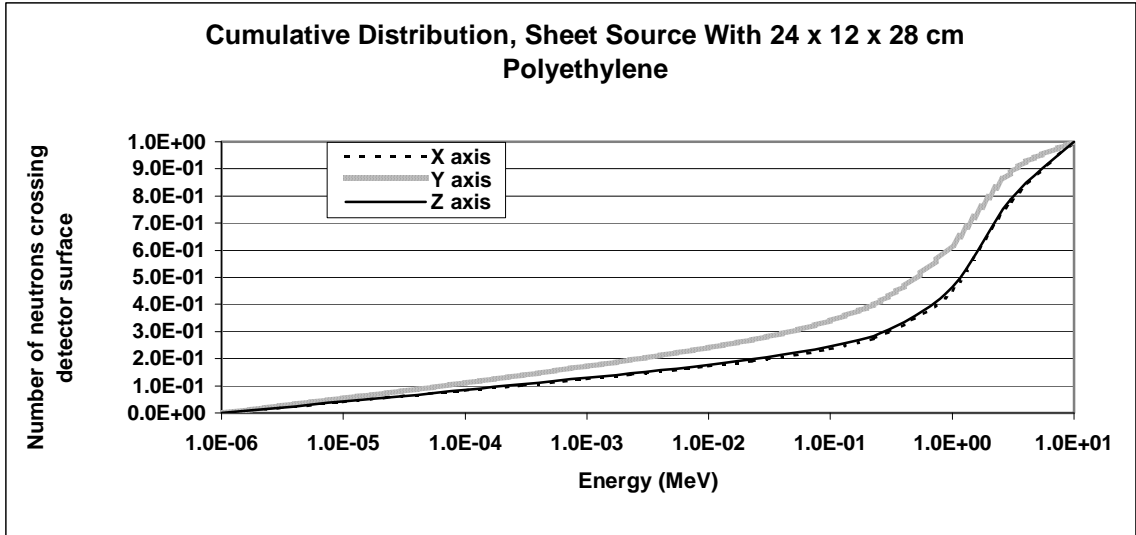


Figure 24. The cumulative distribution for the number of neutrons crossing a flat detector surface of 2500 cm² at a distance of 100 cm from the center of the source along the X, Y and Z axes. The neutrons originate from a 500 g sheet source of uniformly distributed HEU. The source is surrounded by polyethylene with dimensions of 24 x 12 x 28 cm. All data is normalized to 1 neutron particle.

The differences in cumulative distribution for the three axes is compared at energies less than or equal to 1.0×10^{-3} MeV in Table 11. The cumulative distributions are again compared at energies equal to or less than 1.0×10^{-1} MeV. The difference in cumulative distributions for the X and Y axes increases from 4.6% at the 1.0×10^{-3} MeV point to 10.3% at the 1.0×10^{-1} MeV point. The relative error for this data can be found in Table C-8.

Table 11. Comparison of cumulative distributions. The percentage of neutrons crossing flat detector surfaces of 2500 cm² at a distance of 100 cm from the center of the source along the X, Y and Z axes at energies of less than 1.0×10^{-3} MeV and again at energies of 1.0×10^{-1} MeV or lower. The source volumes are a 500 g sheet of uniformly distributed HEU surrounded by polyethylene with dimensions of 24 x 12 x 28 cm of polyethylene shielding.

Comparison of Cumulative Distributions (%)			
Energy (MeV)	X axis	Y axis	Z axis
1.0×10^{-3}	12.5	17.1	12.9
1.0×10^{-1}	23.6	33.9	24.5

The results of the cylinder and sheet source tallies surrounded by 7.5 x 20 x 15 cm of polyethylene were then compared along the X and Y axes (Figure 25).

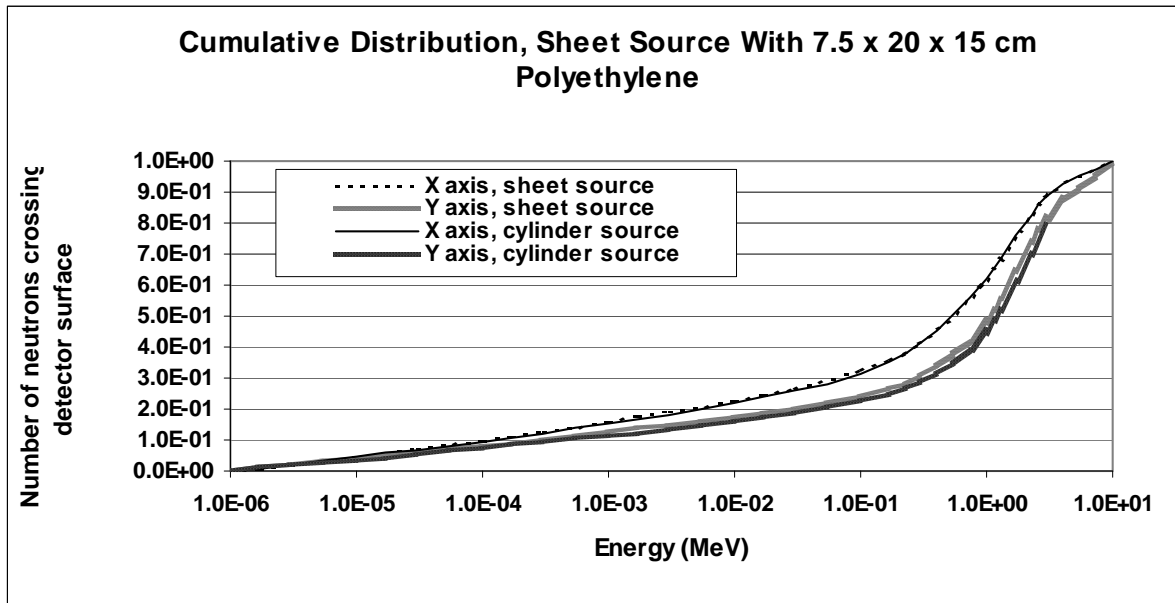


Figure 25. The cumulative distribution for the number of neutrons crossing a flat detector surface of 2500 cm² at a distance of 100 cm from the center of the source along the X and Y axes. The neutrons originate from a 500 g sheet source and a 500 g cylinder source of uniformly distributed HEU. The sources are each surrounded by polyethylene with dimensions of 7.5 x 20 x 15 cm. All data is normalized to 1 neutron particle.

There is a more obvious change in the cumulative distribution for the X axis in the two different configurations than there is for the Z axis. This comparison demonstrates that although the cumulative distributions change from one axis to another, they are very similar between the two configurations. This indicates that the shape of the source volume will have little impact on a source that is surrounded by moderating material.

CONCLUSION

Summary of Results.

Different source volumes were run with various shielding configurations. Each source volume consisted of HEU uniformly distributed throughout the volume. The data was first compared at the surface of a surrounding sphere placed 200 cm from the center of each source volume. In this configuration, no shielding was added. The space between the source volume and the sphere was defined as a void or a vacuum in MCNP. The data from the source volumes were also compared to a Watt spectrum emitted from a point source with no shielding. The cumulative distributions of the neutron current for each source and the point source showed no significant change in the shape of the curve (Table 1). This indicates little to no self-absorption within source volumes of this size.

A 500 g sphere was then surrounded with varying thicknesses of polyethylene shielding (Figure 10). This data indicated that there is an optimal moderation thickness, above which the polyethylene will begin to attenuate the neutrons instead of just moderating them.

The neutron current for a source volume weighing 2000 g was then tallied as a cylinder source and as a sheet source, and compared to HEU sources weighing 500 g (Figure 12). There appears to be no significant shift in the cumulative distribution curve from the 500 g sources to the 2000 g sources at energies equal to and less than 1.0×10^{-3} MeV.

The neutron current was then evaluated at the detector surface along every axis of the basic cylinder configuration for a 500 g source (Figure 6). The detectors were given dimensions of 50 x 50 x 1 cm. Detectors of this size would be manageable in any port of entry and provide acceptable statistics. The X and Y axes were normalized with each other, as they consisted of the same dimensions. The data for the detector surfaces among the different axes at energies equal to and less than 1.0×10^{-3} MeV is almost indistinguishable.

All axes in the basic HEU sheet configuration were then evaluated in the same manner. In this configuration, the X axis surface area is ten times greater than the surface areas along the Y and Z axes so the neutron current along the X axis is expected to be different from the Y and Z axes. The difference in neutron current cumulative distributions becomes more pronounced at energies above 1.0×10^{-3} MeV.

Once the basic configurations were evaluated, polyethylene shielding was added to the model. This moderating material was modeled in such a way as to fit into a suitcase. The first configuration consisted of a cylinder surrounded by a 7.5 x 20 x 15 cm block of polyethylene (Figure 17). The cumulative distribution of the X-axis at and below 1.0×10^{-3} MeV is only slightly higher than that of the Y and Z axes.

The polyethylene shielding dimensions were then modified to 24 x 7 x 28 cm. There was no change in the shape of the cumulative distribution curve. There is a noticeable difference in the cumulative distribution curve for the neutron current along the Y axis detectors and the X and Z axes detectors (Figure 19). This is likely due to the decrease of polyethylene material shielding the source along the Y axis. In this configuration, it seems as though the moderating material is the predominant factor.

Polyethylene was then added to the HEU sheet source (Figure 24). The model was first run with a shielding thickness of 7.5 x 20 x 15 cm and then the dimensions were changed to 24 x 12 x 28 cm. This allowed for evaluation of a slightly different orientation of the shielding material as well as providing data for a different thickness of polyethylene. For the 7.5 x 20 x 15 cm a slight change in the cumulative distribution for energies less than and equal to $1.0 \cdot 10^{-3}$ MeV was noted for the X axis from the Y and Z axes. The difference was more pronounced at energies below the $1.0 \cdot 10^{-1}$ MeV point. When the polyethylene thickness was changed to 24 x 12 x 28 cm, the cumulative distribution along the Y axis shows a notable difference from the cumulative distributions along the X and Z axes (Table 15). In this configuration, the Y axis contains the least amount of moderating material. This shows that as the thickness of the moderator material increases, the moderating material begins to dominate the outcome of the cumulative distribution of the neutron current over the size and shape of the HEU source.

A 500 g cylinder and sheet source with similar polyethylene dimensions were also compared to one another along the X and Z axes. A more pronounced change in the neutron spectrum between the two sources is noted along the X axes as this axes displays a greater difference in moderator thickness than that of the Z axis.

The neutron spectrum was evaluated for several different source geometries with various shielding configurations. A comparison of the results shows that the most significant effect on the neutron spectrum occurs as a result of the moderating material.

The X and Y axes were then compared for the polyethylene configurations with dimensions of 7.5 x 20 x 15cm surrounding the 500 g cylinder and sheet sources (Figure

25). Figure 25 shows that changing the source geometry has little effect on the output while varying moderator thickness around the sources does effect the output.

This data suggest that the shape of the neutron spectrum is more dependent on the material surrounding an HEU source than on the size or shape of that source. At energies less than or equal to 1.0×10^{-3} MeV, the change in cumulative distributions of the neutron current is only slightly distinguishable. The difference between the neutron currents becomes more noticeable as the energy is increased to above 1.0×10^{-1} MeV. This suggests that efforts should focus on a detector design which takes advantage of the similar energy distributions around the 1.0×10^{-3} MeV energy mark.

Future research.

The next step in this process would be to model the different source configurations with various materials in front of the detector surfaces. A material should be selected which can efficiently modify neutrons of approximately 1.0×10^{-3} MeV. Relative error tables in Appendix C show that with any neutron moderation, the statistics in this region are acceptable. Appendix B provides a summary of materials being used in existing fast neutron detectors. These detectors should be examined in greater detail to determine which combination of moderating material and detector volume would provide the most efficient and practical method for detection of neutrons emitted from concealed weapons grade material.

Results of the MCNP modeling show that source size, density, and geometry have a much smaller impact on the outcome of the neutron spectrum than the moderating material. Calculations could be done with varying degrees of shielding thickness in various configurations.

Other more practical configurations should be modeled as well. The International Atomic Energy Agency (IAEA) provides a list of illicit trafficking incidents. This can be found under the title 'Illicit Trafficking Database' or 'ITDB'. It provides a list of the confirmed trafficking incidents along with the material involved and weight of the material. It does not provide exact dimensions of the source material or percent enrichment. Two supplementary tables were provided by the Center for Nonproliferation Studies and 'The Nonproliferation Review' (Monterey Institute of International Studies, 2001, and Potter and Sokova, 2001). These tables provide further information concerning the percent enrichment of the seized material. It would be difficult to replicate the specific scenarios reported in these databases such as the exact dimensions and the circumstances under which the materials were detected due to the classified nature of the information.

An educated guess, however, as to the exact dimensions of a source could be made. One example of a source which was modeled in MCNP but not reported on for this report was an incident concerning the smuggling of a 5 g cylinder of HEU enriched to 70-80% which was confiscated in Paris, France in 2001 (Potter and Sokova, 2002). This cylinder was shielded with a lead lining and found inside the trunk of a car. Without more information available, the HEU cylinder was assigned a density of 18.7 g/cm^3 , and given a radius of 0.25 cm and a height of 1.36 cm. The lead shielding was assigned a density of 11.35 g/cm^3 , and given a radius of 1.25 cm and a height of 2.36 cm.

Another trafficking incident involved an engineer who had been building up his own stockpile of HEU powder from a nuclear research facility that he worked at outside of Moscow over a period of time (Roe, 2003). When the engineer attempted to transport

a suitcase full of the material, he met up with acquaintances at the train station who were wanted for questioning on a burglary. The man was then questioned along with the suspects, and when asked what was in his suitcase, he became nervous and confessed to the police that he was carrying HEU (Roe, 2003). This case of smuggling was detected due to luck and basic human nature. It would be worth replicating this case to determine whether or not a detection system could have alarmed an inspector.

There are also confirmed incidents of stolen ^{239}Pu material. In 1994 police accidentally discovered 6.15 g of ^{239}Pu in an apartment in Germany (Potter and Sokova, 2002). Another case of stolen ^{239}Pu occurred in a Greek village in 2001 (IAEA, 2003). In this case 245 small metal plates containing approximately 3 g of ^{239}Pu were discovered in a buried cache (IAEA, 2003). It is obvious that ^{239}Pu is being acquired with criminal intent, and ^{239}Pu should be modeled in the different configurations as HEU was for this project.

These published incidents show that a smuggler is not always likely to shield weapons grade material with the appropriate material. A neutron detector with a gradient of moderating material would have the ability to detect these types of configurations as well as configurations in which the source volume is shielded.

Confirmed incidents of nuclear material trafficking have shown that likely scenarios may involve source material in the shape of a cylinder or small sheets, and they may be carried in a suitcase or the trunk of a car. Material may also be smuggled in cargo containers at a seaport. This is an attractive method of smuggling material because of the high volume of cargo entering the United States in this manner, making it difficult for customs agents to inspect every package entering the country.

The extensive list of illicit trafficking incidents provided by the IAEA shows the need for an efficient method of detecting weapons grade material. Many case of nuclear smuggling are discovered either through extensive under cover operations or pure luck. The addition of reliable detection systems will not only provide another line of defense, but they will also deter future efforts to smuggle nuclear material.

BIBLIOGRAPHY

Attix, F. H. (1986) *Introduction to Radiological Physics and Radiation Dosimetry*. New York: John Wiley & Sons.

Armed Forces Radiobiological Institute. (1999, January). *Medical Effects of Ionizing Radiation CD-ROM*. Bethesda, MD.

Bias, C. C. (2002). *Optimizing the detection of neutrons from small-quantity weapons-grade nuclear materials*. Unpublished master's thesis, Colorado State University, Fort Collins, Colorado.

Briesmeister, J. F. (2000). *MCNPTM - A General Monte Carlo N-Particle Transport Code, Version 4C Manual*. Los Alamos National Laboratory, Los Alamos, NM.

Cember, H. (1996). *Introduction to Health Physics*. (3rd ed.). NY: McGraw-Hill.

Chang, R. (1988) *Chemistry*. (3rd ed). NY: Random House.

Cochran, R. G., and Tsoulfanidis, N. (1990). *The Nuclear Fuel Cycle: Analysis and Management*. La Grange Park, IL: American Nuclear Society.

Department of Energy and the University of California at Los Alamos National Laboratory (2001). *MCNPTM Version 4C Computer Code*.

Department of Homeland Security. (2003). *U.S. Customs and Border Protection, U.S. Department of Homeland Security. Container Security Initiative*. Retrieved December 9, 2003, from:

http://www.customs.ustreas.gov/xp/cgov/enforcement/international_activities/csi/

Department of Homeland Security. (2003). *U.S. Customs and Border Protection, U.S. Department of Homeland Security. Ports of Entry*. Retrieved December 9, 2003, from: <http://www.customs.ustreas.gov/xp/cgov/toolbox/ports/>

Department of Homeland Security. (2003). *U.S. Customs and Border Protection, U.S. Department of Homeland Security. U.S. Customs and Border Protection Response to Terrorism*. Retrieved December 9, 2003, from: http://www.customs.ustreas.gov/ImageCache/cgov/content/import/cargo_5fcontrol/csi/standard_5fcurrent_5fgeneric_2epps/v1/standard_5fcurrent_5fgeneric.pps

- Duderstadt, J. J., and Hamilton, L. J. (1976) *Nuclear Reactor Analysis*. New York: John Wiley & Sons, Inc.
- Glasstone, S., and Sesonske, A. (1991) *Nuclear Reactor Engineering*. (3rd ed.). Malabar, FL: Krieger Publishing Company.
- International Atomic Energy Agency (2003). *IAEA Illicit Trafficking Database (ITDB)*. Retrieved June 29, 2004 from:
http://www.iaea.org/NewsCenter/Features/RadSources/PDF/itdb_31122003.pdf
- Johns, H. E., and Cunningham, J. R. (1983) *The Physics of Radiology*. (4th ed.). Springfield, IL: Charles C. Thomas Publisher.
- Knoll, G. F. (2000) *Radiation Detection and Measurement*. (3rd ed.). New York, NY: John Wiley & Sons, Inc.
- Lamarsh, J. R. (1983) *Introduction to Nuclear Engineering*. (2nd ed.). Reading, MA: Addison-Wesley Publishing Company.
- Minitab Inc. (1998) Minitab Student Version Release 12 Computer Code.
- Monterey Institute of International Studies. (2001). Retrieved June 29, 2004 from:
<http://cns.miis.edu/pubs/reports/traff.htm>
- Moran, M. J., and Shapiro, H. N. (1988). *Fundamentals of Engineering Thermodynamics*. New York: John Wiley & Sons, Inc.
- National Council on Radiation Protection (2004, April). *Advances in Consequence Management for Radiological Terrorism Events, Fortieth Annual Meeting Abstracts*, Arlington Virginia, April 14-15, 2004. Retrieved April 20, 2004 from:
<http://www.ncrp.com/Prog2004/>
- National Council on Radiation Protection. (2001, October). *NCRP Report No. 138, Management of Terrorist Events Involving Radioactive Material*. Bethesda, MD.
- National Council on Radiation Protection. (1980). *NCRP Report No. 65, Management of Persons Accidentally Contaminated with Radio-nuclides*, Washington, D.C.
- National Institute of Standards and Technology. (2000). *ASTAR database*. Retrieved January 21, 2004 from: <http://physics.nist.gov/PhysRefData/Star/Text/ASTAR.html>
- National Intelligence Council. (2002, February). *National Intelligence Council, Annual Report to Congress on the Safety and Security of Russia Nuclear Facilities and Military Forces*. Retrieved December 9, 2003, from:
http://www.cia.gov/nic/special_russiannucfac.html

Ott, R. L., and Longnecker, M. (2001) *An Introduction to Statistical Methods and Data Analysis*. (5th ed.). Pacific Grove, CA: Duxbury, Thomson Learning.

Potter, W.C., and Sokova, E. (2002, Summer). Illicit nuclear trafficking in the NIS: What's new? What's true? *The Nonproliferation Review*, pp. 112-120.

Roe, S. (2002, January 31). Trafficking in stolen nuclear material on the rise; Experts cite cases since mid-1990s as cause for concern. *Chicago Tribune*. Retrieved June 29, 2004, from: <http://www.cdi.org/russia/191-4.cfm>

Stern, J. (2000). *The Ultimate Terrorists*. (3rd ed.). Cambridge: Harvard University Press.

Turner, J. E., Atoms, (1986). *Radiation, and Radiation Protection*. Elmsford, NY: Pergamon Press.

APPENDIX A

CLASSIFICATION OF NEUTRONS

Neutron classification	Energy (MeV)
Thermal	$0 - 5 \times 10^{-6}$
Slow	$1 \times 10^{-6} - 1 \times 10^{-4}$
Intermediate	$1 \times 10^{-4} - 1 \times 10^{-2}$
Fast	$1 \times 10^{-2} - 10$
High Energy	10 - 500
Relativistic	>500

APPENDIX B

MATERIAL COMPOSITION

Material	Element	Percent Composition (%)	Density (g/cm ³)
Dry air*	Amorphous carbon (6)	0.0124	1.20479 x 10 ⁻³
	Nitrogen (7)	75.5267	
	Oxygen (8)	23.1781	
	Argon (18)	1.2827	
Polyethylene*	Hydrogen (1)	1.4371	0.94
	Carbon (6)	85.6289	

*Data for material compositions were retrieved from (NIST, 2000).

Appendix C

Table C-1. Relative error for configurations without shielding.

Energy region (MeV)	Relative Error (%)			
	Cylinder	Sheet	Sphere	Watt spectrum
0 – 1x10 ⁻⁶	0.00	0.0	0.00	0.00
1x10 ⁻⁶ – 3x10 ⁻⁶	0.00	0.0	0.00	0.00
3x10 ⁻⁶ – 1x10 ⁻⁵	70.71	100.0	58.43	0.00
3x10 ⁻⁵ – 1x10 ⁻⁴	27.33	70.7	20.87	0.00
1x10 ⁻⁵ – 3x10 ⁻⁵	13.04	33.4	11.96	30.15
1x10 ⁻⁴ – 3x10 ⁻⁴	5.59	15.6	5.31	16.22
3x10 ⁻⁴ – 1x10 ⁻³	2.41	7.5	2.33	7.47
1x10 ⁻³ – 3x10 ⁻³	0.98	2.9	0.93	2.97
3x10 ⁻³ – 1x10 ⁻²	0.42	1.3	0.40	1.32
1x10 ⁻² – 3x10 ⁻²	0.16	0.5	0.15	0.52
3x10 ⁻² – 1x10 ⁻¹	0.07	0.2	0.06	0.23
1x10 ⁻¹ – 3x10 ⁻¹	0.03	0.1	0.02	0.09
3x10 ⁻¹ - 1.0	0.01	0.0	0.01	0.04
1.0 - 3.0	0.01	0.0	0.01	0.02
3.0 - 10.0	0.00	0.0	0.00	0.01
Neutron histories tracked	900,000,000	900,000,000	900,000,000	900,000,000

Table C-2. Relative error for 500 g sphere configuration surrounded by spheres of polyethylene.

Energy region (MeV)	Relative Error (%)				
	No polyethylene	5 cm polyethylene sphere	10cm polyethylene sphere	15 cm polyethylene sphere	20 cm polyethylene sphere
0 – 1x10 ⁻⁶	0.00	0.00	0.00	0.00	0.00
1x10 ⁻⁶ – 3x10 ⁻⁶	0.00	0.00	0.00	0.00	0.00
3x10 ⁻⁶ – 1x10 ⁻⁵	58.43	0.12	0.12	0.21	0.35
3x10 ⁻⁵ – 1x10 ⁻⁴	20.87	0.11	0.12	0.20	0.33
1x10 ⁻⁵ – 3x10 ⁻⁵	11.96	0.10	0.12	0.21	0.35
1x10 ⁻⁴ – 3x10 ⁻⁴	5.31	0.09	0.12	0.20	0.33
3x10 ⁻⁴ – 1x10 ⁻³	2.33	0.09	0.12	0.21	0.35
1x10 ⁻³ – 3x10 ⁻³	0.93	0.09	0.12	0.20	0.33
3x10 ⁻³ – 1x10 ⁻²	0.40	0.09	0.12	0.21	0.34
1x10 ⁻² – 3x10 ⁻²	0.15	0.08	0.11	0.19	0.32
3x10 ⁻² – 1x10 ⁻¹	0.06	0.07	0.11	0.19	0.31
1x10 ⁻¹ – 3x10 ⁻¹	0.02	0.06	0.09	0.16	0.26
3x10 ⁻¹ - 1.0	0.01	0.05	0.07	0.12	0.20
1.0 - 3.0	0.01	0.03	0.05	0.08	0.13
3.0 - 10.0	0.00	0.02	0.04	0.06	0.10
Neutron histories tracked	900,000,000	50,000,000	50,000,000	50,000,000	50,000,000

Table C-3. Relative error of neutron tracking data from 500 g cylinder configuration with no shielding.

Energy region (MeV)	Relative Error (%)	
	X +Y axis	Z axis
0 – 1x10 ⁻⁶	0.0	0.0
1x10 ⁻⁶ – 3x10 ⁻⁶	0.0	0.0
3x10 ⁻⁶ – 1x10 ⁻⁵	0.0	0.0
3x10 ⁻⁵ – 1x10 ⁻⁴	0.0	0.0
1x10 ⁻⁵ – 3x10 ⁻⁵	55.9	86.1
1x10 ⁻⁴ – 3x10 ⁻⁴	37.8	55.9
3x10 ⁻⁴ – 1x10 ⁻³	15.8	22.9
1x10 ⁻³ – 3x10 ⁻³	6.8	9.0
3x10 ⁻³ – 1x10 ⁻²	2.9	3.9
1x10 ⁻² – 3x10 ⁻²	1.1	1.4
3x10 ⁻² – 1x10 ⁻¹	0.5	0.6
1x10 ⁻¹ – 3x10 ⁻¹	0.2	0.2
3x10 ⁻¹ - 1.0	0.1	0.1
1.0 - 3.0	0.0	0.1
3.0 - 10.0	0.0	0.0
Neutron histories tracked	900,000,000	900,000,000

Table C-4. Relative error of neutron tracking data from 500 g cylinder configuration with no shielding.

Energy region (MeV)	Relative Error (%)	
	Y + Z axis	X axis
0 – 1x10⁻⁶	0.0	0.0
1x10⁻⁶ – 3x10⁻⁶	0.0	0.0
3x10⁻⁶ – 1x10⁻⁵	0.0	0.0
3x10⁻⁵ – 1x10⁻⁴	0.0	0.0
1x10⁻⁵ – 3x10⁻⁵	25.0	0.0
1x10⁻⁴ – 3x10⁻⁴	0.0	37.5
3x10⁻⁴ – 1x10⁻³	50.6	55.2
1x10⁻³ – 3x10⁻³	25.5	17.4
3x10⁻³ – 1x10⁻²	11.6	8.2
1x10⁻² – 3x10⁻²	4.5	3.2
3x10⁻² – 1x10⁻¹	1.9	1.4
1x10⁻¹ – 3x10⁻¹	0.8	0.6
3x10⁻¹ - 1.0	0.3	0.3
1.0 - 3.0	0.2	0.1
3.0 - 10.0	0.1	0.1
Neutron histories tracked	100,000,000	100,000,000

Table C-5. Relative error of neutron tracking data from 500 g cylinder configuration surrounded by 7.5 x 20 x 15 cm of polyethylene shielding.

Energy region (MeV)	Relative Error (%)		
	X axis	Y axis	Z axis
0 – 1x10⁻⁶	0.0	0.0	0.0
1x10⁻⁶ – 3x10⁻⁶	0.0	0.0	0.0
3x10⁻⁶ – 1x10⁻⁵	0.5	1.2	0.8
3x10⁻⁵ – 1x10⁻⁴	0.4	1.1	0.8
1x10⁻⁵ – 3x10⁻⁵	0.4	1.2	0.8
1x10⁻⁴ – 3x10⁻⁴	0.4	1.1	0.7
3x10⁻⁴ – 1x10⁻³	0.4	1.1	0.8
1x10⁻³ – 3x10⁻³	0.4	1.1	0.7
3x10⁻³ – 1x10⁻²	0.4	1.1	0.7
1x10⁻² – 3x10⁻²	0.4	1.0	0.7
3x10⁻² – 1x10⁻¹	0.3	1.0	0.7
1x10⁻¹ – 3x10⁻¹	0.3	0.8	0.5
3x10⁻¹ - 1.0	0.2	0.6	0.4
1.0 - 3.0	0.2	0.4	0.3
3.0 - 10.0	0.1	0.3	0.2
Neutron histories tracked	75,000,000	75,000,000	75,000,000

Table C-6. Relative error of neutron tracking data from 500 g cylinder configuration surrounded by 24 x 12 x 28 cm of polyethylene shielding.

Energy region (MeV)	Relative Error (%)		
	X axis	Y axis	Z axis
0 – 1x10 ⁻⁶	0.0	0.0	0.0
1x10 ⁻⁶ – 3x10 ⁻⁶	0.0	0.0	0.0
3x10 ⁻⁶ – 1x10 ⁻⁵	0.4	0.8	1.5
3x10 ⁻⁵ – 1x10 ⁻⁴	0.4	0.8	1.4
1x10 ⁻⁵ – 3x10 ⁻⁵	0.4	0.8	1.4
1x10 ⁻⁴ – 3x10 ⁻⁴	0.4	0.7	1.3
3x10 ⁻⁴ – 1x10 ⁻³	0.4	0.8	1.4
1x10 ⁻³ – 3x10 ⁻³	0.4	0.7	1.3
3x10 ⁻³ – 1x10 ⁻²	0.4	0.7	1.3
1x10 ⁻² – 3x10 ⁻²	0.3	0.6	1.2
3x10 ⁻² – 1x10 ⁻¹	0.3	0.6	1.1
1x10 ⁻¹ – 3x10 ⁻¹	0.3	0.5	0.9
3x10 ⁻¹ - 1.0	0.2	0.4	0.8
1.0 - 3.0	0.1	0.3	0.5
3.0 - 10.0	0.1	0.2	0.4
Neutron histories tracked	75,000,000	75,000,000	75,000,000

Table C-7. Relative error of neutron tracking data from 500 g sheet configuration surrounded by 7.5 x 20 x 15 cm of polyethylene shielding.

Energy region (MeV)	Relative Error (%)		
	X axis	Y axis	Z axis
0 – 1x10 ⁻⁶	0.0	0.0	0.0
1x10 ⁻⁶ – 3x10 ⁻⁶	0.0	0.0	0.0
3x10 ⁻⁶ – 1x10 ⁻⁵	0.6	1.3	1.0
3x10 ⁻⁵ – 1x10 ⁻⁴	0.6	1.2	0.9
1x10 ⁻⁵ – 3x10 ⁻⁵	0.6	1.3	0.9
1x10 ⁻⁴ – 3x10 ⁻⁴	0.5	1.2	0.8
3x10 ⁻⁴ – 1x10 ⁻³	0.5	1.3	0.9
1x10 ⁻³ – 3x10 ⁻³	0.5	1.2	0.8
3x10 ⁻³ – 1x10 ⁻²	0.5	1.2	0.8
1x10 ⁻² – 3x10 ⁻²	0.5	1.1	0.8
3x10 ⁻² – 1x10 ⁻¹	0.5	1.1	0.7
1x10 ⁻¹ – 3x10 ⁻¹	0.4	0.9	0.6
3x10 ⁻¹ - 1.0	0.3	0.7	0.5
1.0 - 3.0	0.2	0.4	0.3
3.0 - 10.0	0.2	0.3	0.2
Neutron histories tracked	75,000,000	75,000,000	75,000,000

Table C-8. Relative error of neutron tracking data from 500 g sheet configuration surrounded 24 x 12 x 28 cm of polyethylene shielding.

Energy region (MeV)	Relative Error (%)		
	X axis	Y axis	Z axis
0 – 1x10 ⁻⁶	0.0	0.0	0.0
1x10 ⁻⁶ – 3x10 ⁻⁶	0.0	0.0	0.0
3x10 ⁻⁶ – 1x10 ⁻⁵	1.7	0.6	0.0
3x10 ⁻⁵ – 1x10 ⁻⁴	1.6	0.6	0.0
1x10 ⁻⁵ – 3x10 ⁻⁵	1.7	0.6	0.0
1x10 ⁻⁴ – 3x10 ⁻⁴	1.6	0.6	0.0
3x10 ⁻⁴ – 1x10 ⁻³	1.7	0.6	0.0
1x10 ⁻³ – 3x10 ⁻³	1.6	0.6	0.0
3x10 ⁻³ – 1x10 ⁻²	1.6	0.6	0.0
1x10 ⁻² – 3x10 ⁻²	1.5	0.5	0.0
3x10 ⁻² – 1x10 ⁻¹	1.5	0.5	0.0
1x10 ⁻¹ – 3x10 ⁻¹	1.2	0.4	0.0
3x10 ⁻¹ - 1.0	1.0	0.3	0.0
1.0 - 3.0	0.6	0.2	0.1
3.0 - 10.0	0.4	0.2	0.1
Neutron histories tracked	75,000,000	75,000,000	75,000,000

APPENDIX C

FAST NEUTRON DETECTORS

Detector	Cons	Pros	Limitations
Detectors based on neutron moderation			
Bonner spheres	Small LiI scintillator placed in the middle of polyethylene moderating spheres.	<ul style="list-style-type: none"> -Provides information on the incident neutron energy distribution. -high Q-value of Li capture reaction allows for effective gamma ray discrimination. 	<ul style="list-style-type: none"> -Below 100 KeV direct measurements of detector efficiency are unreliable. -Moderating process eliminates neutron energy spectrum information. -Detection process is relatively slow (10s - 100s of μs).
Leake dosimeter	Spherical neutron dosimeter similar to Bonner spheres. LiI scintillator is replaced with ^3He proportional counter. A spherical Cd absorber with perforated holes is placed around ^3He .	<ul style="list-style-type: none"> -Higher gamma ray discrimination capability. -Response to shielded fission sources deviates by $<\pm 40\%$. 	<ul style="list-style-type: none"> -Over responds to neutrons in the KeV range. -Moderating process eliminates neutron energy spectrum information. -Detection process is relatively slow (10s - 100s of μs).
Flat response detectors using BF_3	BF_3 tube placed in the center of a moderator	<ul style="list-style-type: none"> -Does not depend strongly on neutron energy. -Flat energy response of the detector. -Holes on front surface panel prevent reduction of efficiency for 	<ul style="list-style-type: none"> -Directional dependency. -Detector efficiency of 0.25%. -Moderating process eliminates neutron energy spectrum information.

		neutrons < 1 MeV. -Amplitude discrimination allows for elimination of gamma ray interference. -Good long-term stability.	-Detection process is relatively slow (10s - 100s of μ s).
Flat response detectors using ^3He	^3He gas replaces BF_3 in the detection tube. Five separate detectors are located near the center of a cylindrical moderating material.	-Higher neutron detection efficiency of 11.5%.	-Moderating process eliminates neutron energy spectrum information. -Detection process is relatively slow (10s - 100s of μ s).
Grey neutron detector	NaI(Tl) scintillator detects 2.2 MeV capture gamma rays when neutrons are thermalized in a hydrogenous sphere.		-Moderating process eliminates neutron energy spectrum information. -Detection process is relatively slow (10s - 100s of μ s).
Black neutron detector	Uses light produced in a hydrogenous spherical scintillator as neutrons are moderated	-Faster response time.	-Moderating process eliminates neutron energy spectrum information. -Detection process is relatively slow (10s - 100s of μ s).
Detectors based on fast neutron-induced reactions- incident neutron energy can be determined from by subtracting the total kinetic energy of reaction products from the Q-value of the reaction.			
$^6\text{Li}(n,\alpha)$ reaction methods	-Reaction drops off smoothly with increasing neutron energy except in resonance region.	Q= 4.78 MeV reaction allows better detection of thermal neutrons.	Q= 4.78 MeV reaction degrades detection of fast neutrons because of competing $^6\text{Li}(n,n'd)^4\text{He}$ reaction. In this reaction, an unwanted

<p><i>LiI scintillator</i></p>			<p>neutron is produced which will effect detection.</p> <p>-Additional energy peak may be noticed in detection due to moderation from walls, shielding, etc.</p> <p>-At room temperature, nonlinearity response to tritons and alpha particles degrades detector response. This leads to an energy peak resolution of 40%.</p>
<p><i>LiI glass scintillator-</i></p>	<p>granular scintillators consist of mixtures of LiF and ZnS. Silicate glass with Cerium activation are used as a medium.</p>	<p>-Resolution can be improved to a full energy peak of 20% by cooling crystals to liquid nitrogen temperature. The practicality of cooling to this degree is difficult.</p> <p>-High response time.</p>	<p>-Poor light output and nonlinearity response.</p> <p>-Poor gamma ray discrimination.</p>
<p><i>Li glass fiber scintillators-</i></p>	<p>-Glass scintillators are shaped as small diameter optical fibers.</p>	<p>-Glass fibers containing enriched ^6Li – electrons produced by gamma emission have a reduced energy deposition in material due to small diameter.</p> <p>-Diameter of 100 μm improves gamma ray discrimination.</p> <p>-Terbium substituted as an activator may provide better light transmission. It has a lower fluorescent decay time of 3 ms.</p>	<p>-Cerium doped glass produces a detection discrepancy because of an overlap of the Ce^{3+} fluorescence sites with the absorption of Ce^{4+} atoms when oxidation of Ce occurs.</p>

<p><i>Li sandwich spectrometer</i></p>	<p>-Thin layer of LiF is prepared on thin backing and placed between 2 semi-conductor diodes. Reaction products are oppositely directed and coincident pulses are observed.</p>	<p>Less optical self absorption occurs, so longer optic fibers may be used.</p> <p>-Determine incident neutron energy by calculating the sum of the coincident energy pulses and subtract the Q-value of the Li reaction.</p> <p>-Coincidence detection reduces background interference.</p>	<p>-Energy losses occur in target material.</p> <p>-As target material is made thinner, counting efficiency is decreased.</p> <p>-Reaction products may not be exactly opposite. Coincidence detection is reduced as neutron energy increases.</p>
<p>Detectors based on the $^3\text{He}(n,p)$ reaction- Fast neutron cross section decreases rapidly as neutron energy increases. Elastic scatter of neutrons from He nuclei produces competing process. Full energy of reaction products is totally absorbed within the detector. Full energy peak is observed for (n,p) reactions caused by incident neutrons. Pulse height continuum results from elastic scatter of neutrons and transfer of energy to He recoil nucleus. Epithermal peak appears as a result of neutron moderation from external materials.</p>			
<p>He³ proportional counter</p>	<p>Krypton added to He gas to reduce reaction product ranges.</p>	<p>-Short rise time of recoil events leads to better discrimination.</p>	<p>-Wall effect reduces detection efficiency.</p>
<p>He³ ionization chamber</p>	<p>Operate as gridded ionization chambers.</p>	<p>-Better pulse height resolution than proportional counter.</p> <p>-Good energy resolution for fast neutrons.</p>	<p>-Slow pulse collection time and small pulse amplitude.</p> <p>-Long pulse shape times required (5-10 μsec).</p>
<p>He³ scintillator</p>		<p>-Fast rise time of output pulse.</p>	<p>-Poor light yield.</p> <p>-Poor pulse height resolution.</p>
<p>Detectors that use fast neutron scatter- Based on elastic scatter of neutrons by light nuclei. Recoil nucleus loses energy as it travels the detection medium. Hydrogen is the most efficient material for this reaction and it produces recoil protons. Q-value of</p>			

reaction equals zero, so incident neutron energy can be determined through energy of recoil proton.			
Proton recoil scintillators		<p>-Stilbene crystals allow for high gamma ray rejection rate.</p> <p>-Gamma rays travel at the speed of light, fast neutrons travel at 5% of the speed of light. Some efforts are being made to exploit this effect.</p>	<p>-Crystals are difficult to obtain and expensive.</p> <p>-Directional variation of light output in crystals.</p> <p>-Scintillator size must be kept small. Counting efficiency decreases as material thickness decreases. Resolution decreases material thickness increases.</p> <p>-Nonlinear light output distorts proton energy distribution.</p> <p>-Some proton recoil events are eliminated by discrimination process.</p>
Gas recoil proportional counters	Hydrogen containing low Z material such as Methane or Helium. Proton recoil spectrum will have a rectangular shape.	-Neutron induced pulses have shorter rise times than gamma ray induced pulses.	<p>-Lower counting efficiency than organic scintillators.</p> <p>-Microscopic air leaks lead to detector failures.</p> <p>-High gamma ray sensitivity.</p>

(Knoll, 2000)